A MICROELECTRODE STUDY OF CORAL CALCIFICATION

HOW OCEAN ACIDIFICATION AFFECTS ION CONCENTRATIONS INSIDE CORAL POLYPS

by

Yuening Ma

A thesis submitted to the Faculty of the University of Delaware in partial fulfillment of the requirements for the degree of Master of Science in Marine Studies

Fall 2015

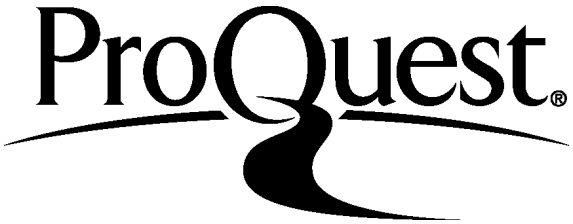

A MICROELECTRODE STUDY OF CORAL CALCIFICATION

HOW OCEAN ACIDIFICATION AFFECTS ION CONCENTRATIONS

INSIDE CORAL POLYPS

by

Yuening Ma

Approved: _____

Wei-jun Cai, Ph.D.
Professor in charge of thesis on behalf of the Advisory Committee

Approved: _____

Mark A. Moline, Ph.D.
Director of the School of Marine Science and Policy

Approved: _____

Mohsen Badiey, Ph.D.
Acting Dean of the College of Earth, Ocean, and Environment

Approved: _____

Ann L. Ardis, Ph.D.
Interim Vice Provost for Graduate and Professional Education

ACKNOWLEDGMENTS

I wish to thank all of the people who guided me, helped me, or encouraged me during this work.

My deepest gratitude goes to adviser, Dr. Wei-jun Cai, who spend years teaching me, reading papers with me and helping me solving problems when my research stocked, encouraged me when I feel depressed for bad result;

Second, I would like to express my gratitude to my two co-advisors, Dr. Brian Hopkinson and Dr. Mark Waner. Dr. Brian Hopkinson, who leads me to the world of marine biology and showed me the attitude to be a professional scientist; Dr. Mark Waner, who helped me with many questions and expanded my view with many interesting articles. I learned a lot from such a acknowledge person.

Special thanks to my friends and colleagues: Qian Ding, Anna Tansik, Wei-jen Huang, Shiyu Wang, Andrew Joseph, Yuanyuan Xu, and Yonghui Gao.

TABLE OF CONTENTS

LIST OF TABLES

LIST OF FIGURES

ABSTRACT

Coral reefs are a critical building block of the ocean ecosystem, whose health is threatened by ocean acidification (OA) and warming due to increased atmospheric CO_2 (Hoegh-Guldberg, 2010; IPCC, 2014). Reliably predicting how coral calcification may respond to OA depends on our understanding of their calcification mechanisms (Ries, 2011; Holcomb et al., 2014; Allison et al., 2014; Gagnon, 2013). But obtaining relevant data on the calcification mechanism is difficult. First, because of coral's structural arrangement, little is understood about the chemical dynamics inside coral polyps. Second, the speciation, sources, and dynamics of dissolved inorganic carbon (DIC) inside corals remain unresolved because only pH has been measured while a critical second parameter needed to fully characterize the internal carbonate chemistry at the site of coral calcification has been missing (Ries, 2011). Coral calcification processes are affected by changes in ion concentrations due to ocean acidification. Microsensors enable us to measure biological processes in different localities of the coral polyp and we have successfully built pH, CO_3^{2-}, and Ca^{2+} microelectrodes that are suitable for coral studies with a tip diameter of 10-15 μm. Also this research is the first to combine pH and CO_3^{2-} to calculate DIC inside coral polyp.

Two chapters are included in this thesis: chapter 1 focuses on pH and CO_3^{2-}concentrations inside calcifying fluid and chapter 2 focuses on the effects of light on Ca^{2+} , CO_3^{2-}, and pH dynamics inside coral polyps and different factors that affect the concentration change.

In chapter 1, we report the first depth profiles of pH and carbonate ion concentrations ($[CO_3^{2-}]$) measured inside coral polyps. We observed sharp increases in pH and $[CO_3^{2-}]$ inside the calcifying fluid and very low pH and $[CO_3^{2-}]$ above it in the coelenteron, supporting the existence of an active process that pumps protons (H^+) out of the calcifying fluid. This results in a sharp CO_2 gradient from the coelenteron to the calcifying fluid, which draws in enough CO_2 to sustain the high calcification rates typically observed in tropical corals (Alison et al, 2014; Furla et al., 2000). However, in contrast to the current view that corals substantially concentrate both DIC and total alkalinity (TA) in their calcifying fluid (Allison et al., 2014), our data and model calculations suggest that corals can achieve a high aragonite saturation state (Ω_{arag}) by maintaining a high pH while at the same time keeping [DIC] and TA relatively low. Such a state requires less H^+-pumping for upregulating pH compared to a high [DIC] scenario.

In chapter 2, the effects of light on Ca^{2+} , CO_3^{2-}, and pH dynamics were measured by microelectrodes inside the polyps of two scleractinian corals, *Orbicella faveolata* and *Turbinaria reniformis*. In the upper part of the coelenteron solution, pH and CO_3^{2-} both increased in the light and decreased in the dark. Ca^{2+} concentrations decreased in the light and increased in the dark. pH and Ca^{2+}

dynamics have been studied in many other studies but no one has yet measured CO_3^{2-} concentrations. Now with our CO_3^{2-} data, we can get a better understanding of carbonate system dynamics over light/dark cycles. Based on our pH and CO_3^{2-} data, we calculated the total alkalinity (TA) and dissolved inorganic carbon (DIC) dynamics and set up a numerical simulation model to analyze the effects of different parameters. The model incorporated calcification, photosynthesis, respiration, physical diffusion with seawater, transmembrane ion transport by Ca-ATPase, and paracellular ion fluxes. Our model was based on the model of Nakamura et al., (2013) and our experimental data (e.g., depth, calcification rate, alkalinity and DIC concentrations) were used to replace some tuning parameters. In our experiment, we found that both TA and DIC decreased in the light and increased in the dark. Our model showed that: 1) Most of the TA and DIC increase in dark were due to physical diffusion from overlying seawater; 2) There are unknown TA sources inside coral polyp that provided about 40% TA in dark, about 15% of that come from inorganic sources; 3) TA and DIC decreases in the light were driven by calcification and photosynthesis. The model agreed with the trends in our experimental data and allowed us to constrain the ratio of different parameters.

Chapter 1

CORALS CONCTROL THEIR INTERIOR PH AND CARBONATE CHEMISTRY AS REVEALED BY MICROELECTRODE PROFILES

1.1 Introduction

Atmospheric CO_2 has increased from 280 parts per million (ppm) during pre-industrial time to 400 ppm today(IPCC, 2014). This CO_2 increase in the atmosphere has caused greater CO_2 dissolution in the ocean, which has modified the DIC species composition in seawater such that proton concentration (i.e., $[H^+]$) has increased, and surface ocean pH level and $[CO_3^{2-}]$ has decreased; a process popularly known as ocean acidification (OA) (Caldeira and Wickett, 2003; Orr et al., 2005). The decrease in $[CO_3^{2-}]$ is particularly detrimental to the health of coral reef organisms and its associated ecosystem functions and biogeochemical processes (Langdon et al., 2003; Hoegh-Guldberg, 2010), because OA leads to decreases in calcification in many, though not all reef species (Hoegh-Guldberg, 2010; Ries, 2011; Shamberger et al., 2014). To understand and predict how corals might respond to current and future CO_2 increases and OA, we need to better understand the coral calcification mechanism, particularly the sources and speciation of DIC that sustain calcification inside the calcification medium (Ries, 2011; Cohen and Holcomb, 2009; Allison et al., 2004; Venn et al., 2011; Holcomb et al., 2014). Despite decades of research, our knowledge

on the internal carbonate chemistry of corals is still limited and direct evidence is still needed to constrain coral calcification mechanisms.

In order to precipitate $CaCO_3$, corals must be able to import Ca^{2+} ions and DIC from seawater, but the import processes remain poorly understood and controversial. Although proposed routes of ion import differ in their details, potential import processes can be broadly grouped into three categories: 1) transmembrane active transport, 2) paracellular diffusion, and 3) whole seawater import (Allemend et al., 2004; Tambutte et al., 2015; Gagnon et al., 2012). Which of these three processes dominates the import pathway for DIC remains unknown because a complete characterization of the internal carbonate chemistry of corals is lacking. To keep the charge balance, a coral must also export H^+ from its interior calcifying space, which also creates a high pH and, by chemical equilibrium, high CO_3^{2-} concentration, and aragonite saturation state inside the coral calcification medium, thus promoting $CaCO_3$ precipitation there. This theoretical understanding of coral calcification is considered the foundation for hypotheses of how calcification will respond to future acidification (Ries, 2011), yet lacks the necessary direct measurements to fully substantiate this theoretical mechanisms of calcification in corals.

Microelectrodes are a powerful technique for the direct measurement of chemical concentrations within organisms such as corals. Previous coral studies have primarily used pH microelectrodes and have shown that pH increases near the coral surface and in the upper region of the polyp's gastric cavity due to photosynthesis but

decreases deeper in the coelenteron due to respiration (Kuhl et al., 1995). Most importantly, very high pHs (8.7–10) have been measured in the calcifying medium using pH microelectrodes and pH sensitive dyes (Ries, 2011; Venn et al., 2011; Al-Horani et al., 2003). These experiments show corals export protons from the calcifying medium to achieve a high $CaCO_3$ saturation state, which facilitates rapid rates of calcification. However, to characterize the internal carbonate chemistry fully, pH alone is not sufficient and another carbonate system parameter should be measured.

1.2 Result

In this work, we used both pH (Han et al., 2014; Cai et al., 2000; Zhao et al., 1999) and CO_3^{2-} microelectrodes (de Beer et al., 2008; Han et al., 2014) to profile the interior of coral polyps through the mouths (see Meth ods below). We advanced a microelectrode inside the polyp's gastric cavity at a resolution of 50 μm per step (5 μm in one case) parallel to the polyp wall until it was broken on the solid $CaCO_3$ base (Figure 1-1a & b). Duplicate micro-profiles measurements revealed that the profiles were reproducible (Figure. 1-1b) even though polyp contraction may shift the relative depth (Figure A2).

We obtained several full-depth profiles of pH and CO_3^{2-} through the polyp mouth, the coelenteron, and into the calcifying medium for three tropical coral species: *Orbicella faveolata* (previously *Montastrea faveolata*), *Turbinaria reniformis*, and *Acropora millepora*. For *O. faveolata*, two pH profiles were recorded,

one in a long polyp of about 2.6 mm and one in a short polyp of about 1.3 mm (Figure 1-2a) while [CO_3^{2-}] was recorded in one short polyp of about 1.2 mm (Figure 1-2b). In these cases, pH increased from 8.1 and [CO_3^{2-}] from 180 μM in the overlying water to 8.3-8.5 and 300 μM respectively in the upper part of the polyp in response to photosynthesis. Deeper in the polyps, pH decreased to a value of 7.7 as a result of respiration, confirming earlier reports (Kuhl et al., 1995). Correspondingly, [CO_3^{2-}] decreased to a value of 100 μM. Then, within a short distance, pH increased sharply to as high as 9.7 while [CO_3^{2-}] increased to 600 μM before the electrode tips broke. We interpret this rapid increase in pH and [CO_3^{2-}] as evidence that the microelectrodes made measurements within the calcifying medium prior to breaking.

Similar but variable profiles were measured inside coral polyps of *T. reniformis* with pH in the calcifying medium being 8.8 to 10.2 (Figure 1-2c) and [CO_3^{2-}] being 1000-1400 μM (Figure 1-2d). In the case of the *A. millepora* polyp, the electrode advancement step was reduced to 5 μm producing a very fine scale pH profile showing a sharp increase in pH from 8.15 to 8.65 within only a short distance of 15-55 μm (Figure 1-2c). Similarly, we observed an increase in [CO_3^{2-}] from as low as ~100 μM in coelenteron to as high as >1500 μM in the calcifying medium within a distance of ~50 μm in *A. millepora* (Figure 1-2d). Our microelectrode profiles of pH and [CO_3^{2-}] confirm early assertions that corals maintain a high pH in their interior environment that allows $CaCO_3$ formation. Moreover, the first ever measured [CO_3^{2-}] profiles reported here demonstrate that [CO_3^{2-}] (500 to 1500 μm) and aragonite

mineral saturation state (Ω_{arag} = 8-24) (Table A4) inside the calcifying medium are high, which is generally consistent with inorganic $CaCO_3$ formation experiments (Cohen and Holcomb, 2009) or previously proposed model frameworks (Ries, 2011; Venn et al., 2011).

We were only able to collect data in the calcifying medium a few times out of numerous profiles on these coral species, most likely because the calcifying medium layer is very thin and isolated in pockets (Venn et al., 2011; Gagnon, 2013). In most cases, the electrode tips broke in one step (50 μm) between the bottom of the polyp gastric cavity space (coelenteron solution) and the hard $CaCO_3$ base, but in some cases the data suggests the calcifying medium is much thicker than previously thought (up to 100 μm). Alternatively, it is possible that the newly formed $CaCO_3$ minerals are porous allowing the glass microelectrode tip to penetrate slightly or that the microelectrode may bend under force after contacting the skeleton thus giving an unrealistic measure of the calcifying medium thickness. Nonetheless a high pH and high [CO_3^{2-}] layer is unequivocally detected in the calcifying medium, though further work is needed to better define its thickness. Our methods do not allow simultaneous profiling of pH and [CO_3^{2-}] at the same depths. Therefore, we constructed composite profiles of pH and [CO_3^{2-}] based on the range of our data across all three species and calculated DIC, TAlk, [CO_2] and Ω_{arag} profiles (Table A4).

Carbonate chemistry compositions through the coelenteron and into the calcifying medium are thus presented here alongside a conceptual model for coral

calcification (Figure 1-3). Our study shows that as pH and [CO_3^{2-}] increase near the polyp surface and in the upper part of the coelenteron (Figure 1-1b, 2), DIC decreases slightly relative to seawater values due to photosynthetic CO_2 consumption (Figure 1-3). Next, DIC increases due to respiratory input of CO_2 and reaches a peak at the bottom of the coelenteron before rapidly declining again in the calcifying space (Figure 1-3b). TAlk in coelenteron is nearly constant throughout most of the gastric cavity space, but decreases slightly at the base of the coelenteron as a result of proton pumping from the calcifying tissue and medium below, then increases dramatically in the calcifying medium. Nonetheless, DIC and TAlk values in the coelenteron solution are not greatly different from those of the overlying seawater, similar to a direct TAlk measurement (Agostini et al., 2012). What is most conspicuous is a sharp increase in CO_2, [CO_2], to ~30 μmol/kg toward the bottom of the coelenteron solution (Figure 1-3b). This increase not only is due to respiration-induced DIC increase but also is greatly enhanced by a simultaneous TA decrease. Thus, we attribute this [CO_2] increase to the conversion of HCO_3^- by H^+ exported from the calcification fluid to CO_2 (Figure 1-3a), a process that requires enzyme carbonic anhydrase. Inside the calcifying medium, the [CO_2] is nearly zero (Figure 1-3b), primarily due to the high pH there (Figure 1-2a, c). This very high CO_2 concentration gradient (~30 μmol/kg, Table A1) would drive a high rate of CO_2 molecular diffusion from coelenteron through the tissue into the calcifying medium, providing an essential source of inorganic carbon for $CaCO_3$ precipitation.

We can estimate CO_2 flux either by a 1-D diffusion model or by an exchange coefficient between two "boxes," the coelenteron and the calcifying medium (equations given in Methods and Table A4 for details). Based on the pH and $[CO_3^{2-}]$ profiles, we determined that the distance between the measured $[CO_2]$ gradient is on the order of 50-100 μm (even though the thickness of the calicoblastic epithelium is probably thinner) and assume that the seawater diffusion coefficient (Li and Gregory, 1974) is applicable. As such, the estimated CO_2 diffusion flux is as high as 51.5-103 mmol $m^{-2}d^{-1}$ (or 217-433 nmol $cm^{-2}h^{-1}$). Alternatively, using the CO_2 exchange coefficient determined by an isotopic tracer method (Agostini et al., 2012; Hohn and Merico, 2012), the CO_2 influx is estimated as 20-72 mmol $m^{-2}d^{-1}$ (82-301 nmol $cm^{-2}h^{-1}$). These CO_2 sink flux estimates compare favorably with coral calcification rates measured in the past (150 to 1500 nmol $cm^{-2}h^{-1}$) (Allemend et al., 2004; Barnes and Devereux, 1984). Thus, the sharp CO_2 depth profile determined here (Figure 1-3b) provides the first direct empirical evidence that DIC produced by respiration in the coelenteron is transported as CO_2 into the calcification fluid. We further suggest that the coral's proton pumping ability is essential not only for creating a high aragonite saturation state in the calcifying medium favoring calcification but also for creating a low pH condition at the bottom of the coelenteron facilitating inorganic carbon influx to support calcification. The latter is reflected by the high ratio of $[CO_2]$ to DIC in the coelenteron above calicoblastic epithelium (i.e., as high as 12%) compared to the much lower ratio in seawater (i.e., 0.47%). This CO_2 transport mechanism supports an earlier study that used radiotracers to show that respired CO_2 is an important source of

DIC for calcification (Furla et al., 2008). Although not mutually exclusive, our passive CO_2 transport mechanism removes the need for the active transport of HCO_3^- either by active transport proteins such as carbonic anhydrase or by vacuoles and inter-cellular channels.

Despite the great CO_2 flux across the calicoblastic epithelium, our analysis reveals that the DIC inside coral calcifying medium is depleted or not much different from seawater (within 20%) due to the consumption of inorganic carbon during calcification, which balances the CO_2 influx (Figure 1-3). Similarly, calcifying medium TAlk increases only moderately compared to outside seawater TAlk (i.e., 1 to 2 times). Earlier attempts to assess the aragonite saturation state of the calcifying medium used pH values (the only measured carbonate parameter) but assumed that DIC and TAlk would be greatly elevated above seawater concentrations due to DIC import, respiration, and proton export (Furla et al., 2000;Caldeira and wicket, 2003; Orr et al., 2005). Our direct [CO_3^{2-}] measurement shows that while aragonite saturation state inside the calcifying medium is elevated, DIC is low and TAlk is only moderately elevated from the background seawater. Thus, achieving a high CO_3^{2-} concentration (and consequently a high aragonite saturation state) can be accomplished without the energetically costly import of HCO_3^- and without TAlk greatly above seawater concentrations, as had been previously assumed. These conclusions are valuable to our understanding and modeling of coral calcification and its response to future ocean acidification. Further research is needed to confirm the pH

and [CO_3^{2-}] profiles with a better spatial resolution, to narrow down the DIC and TAlk ranges inside the calcifying medium, and to confirm our results in other coral species.

1.3 Methods

Details of coral collection and tank incubation conditions are given in the Supplement section I. Method details of making the microelectrodes and their calibration and stability evaluation are given in literature (Han et al., 2014; Cai et al., 2000; Zhao et al., 1999). Additional microelectrode fabrication details specific to this study are giving in the Supplement section II. Details of the microelectrode profiling methods and experiment setup are given in the Supplement section III. In brief, a coral branch was transferred from the incubation tank together with the tank water into the small measurement chamber which was kept at 26°C. The coral branch was allowed to sit in the small container for 1-2 hours until the microelectrode reading was stable in the chamber water (Figure A2). While pH and CO_3^{2-} microelectrodes were calibrated right before use, chamber water pH measured by the large commercial electrode and measured TAlk value were used as the reference point before coral profiling. Under the microscope, one could observe, the coral react and close its mouth when the microelectrode tip entered the polyp cavity space. This depth was marked as the boundary and recorded as a polyp depth of 0 μm. Then the electrode was advanced down progressively at preset step of 5-50 μm until it was broken and a relatively stable pH reading was recorded at each step. The pH reading was considered

as stable if drift was <0.003 pH/min or a total of 3 min, whichever was first. A 3 min limit was established because in some cases, completely stable pH was not realistic due to constant changes in biology.

To check if the electrode maintained function during a profile measurement, a microelectrode was pulled out to the overlying seawater and checked (Figure 1-1b and Figure A2e). Then, the microelectrode was again brought inside the polyp mouth and advanced farther down the polyp until microelectrode broke from hitting the hard base of the $CaCO_3$ skeleton and produced a noise-free and constant voltage reading.

Using directly measured pH and $[CO_3^{2-}]$, we calculated concentrations of other DIC species and the total alkalinity (TAlk) as well as the CO_2 flux as described in the Supplement section IV.

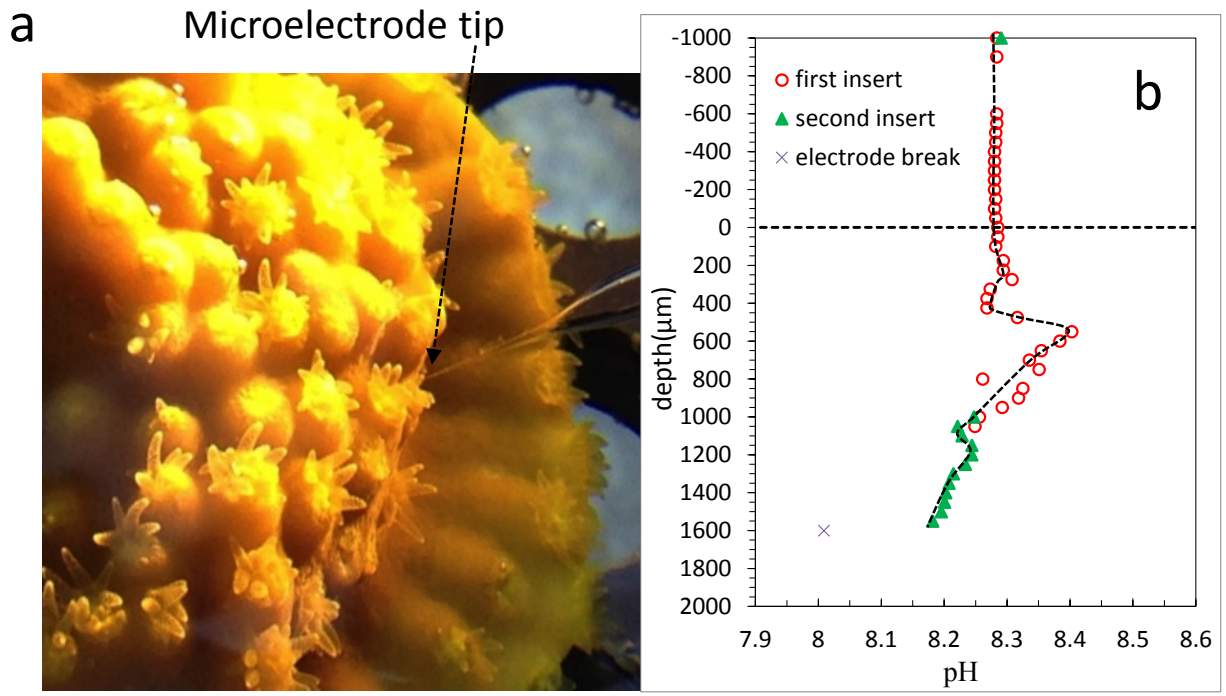

Figure 1-1 Microelectrode profiling and electrode performance. a) Close-up views of the coral Turbinaria reniformis showing the tip of a microelectrode as it enters the polyp. (b) Repeated pH microelectrode profile readings inside a T. reniformis coral polyp. (c) Repeated pH microelectrode profile readings inside an Acropora millepora coral polyp. Between the last point of the second insert and next reading (which is a noise-free reading and is marked as x), the microelectrode tip broke.

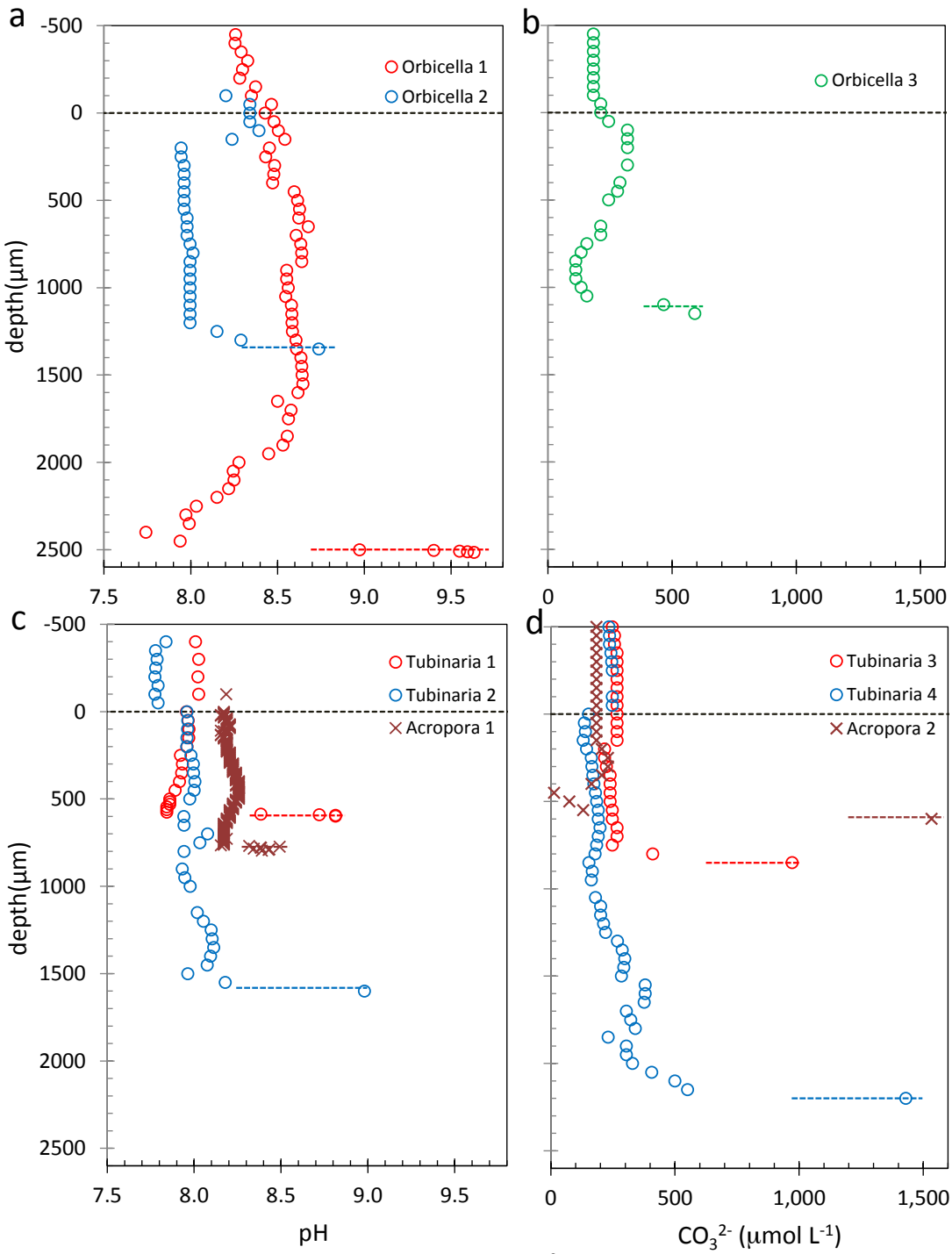

Figure 1-2 Coral internal pH (a) and $[CO_3^{2-}]$ (b) through the polyp mouth of an *Orbicella faveolata* and coral internal pH (c) and $[CO_3^{2-}]$ (D) through the polyp mouth of a *Turbinaria reniformis* and an *Acropora millepora* coral. Each profile was

collected separately at a different time and from different polyp mouths. Dashed black lines indicate the top of the polyp mouths. Colored dashed lines roughly indicate the location of the transition from the basal tissue layer and the calcifying fluid and differ in depth for each polyp.

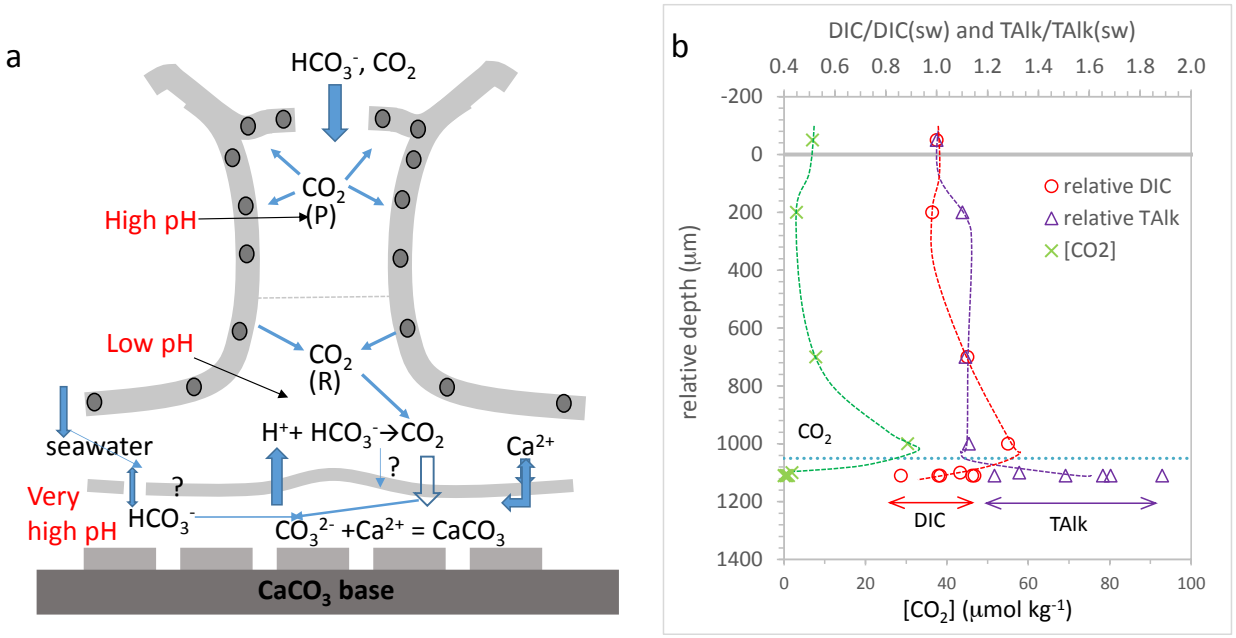

Figure 1-3 (a) Conceptual model of coral calcification, CO_2 transport mechanism, and distributions of internal [CO_2], DIC and TAlk. Dark circles are photosynthetic endosymbionts. (b) For DIC (red line) and TAlk(purple line), calculated ranges of possible concentrations are provided based on calculations of all species from Table A4. The boundary between the base of the coral tissue and the calcifying medium is showed with a blue dashed line. As DIC and TAlk in seawater in our incubation tank varied quite a bit, the ratios of internal to external concentrations are presented. DIC = dissolved inorganic carbon, Talk = total alkalinity.

Chapter 2

A MODEL ON LIGHT EFFECTED CARBON SYSTEM INSIDE THE GASTRIC CAVITY CORAL *ORBICELLA FAVEOLATA* AND *TURBINARIA RENIFORMIS*

2.1 Introduction

Atmospheric CO_2 has increased by approximately 100 ppm since the beginning of the industrial revolution. The ocean has absorbed about 30% of this CO_2 emitted by fossil fuel burning (Sabine et al., 2004), which lead to a series of chemical change including a drop in pH, a decrease of carbonate concentration (CO_3^{2-}), and a lower saturation state for calcium carbonate minerals (Ω; Orr., 2011). Climate change due to the release of CO_2 threatens many marine organisms today; corals are one species among them as they could have difficulties in producing $CaCO_3$ skeleton as the saturation state for aragonite drops (Hoegh-Guldberg et al., 2007).

Scleractinian corals live in a symbiotic relationship with the dinoflagellate Symbiodinium sp. (zooxanthellae). Photosynthesis, respiration, and calcification are the dominant physiological processes of the coral holobiont. The coral polyp has a "bag structure" with two single-celled layers, which is separated by mesoglea. The oral layer ectoderm and aboral layer endoderm lines the coelenteron, in which the fluid could exchange with surrounding seawater through the opened mouth (Barnes

and Chalker, 1990). The cell layer overlying the coral skeleton that is involved in the production of coral skeleton is termed the calicoblastic epithelium. The calcifying fluid, from which new skeleton is precipitated, exists between the skeleton and the calicobalstic epithelium (Johnston, 1980).

Many studies have focused on the macro scale of coral reefs, such as reef metabolism (e.g., Gattuso et al., 1996). But because of the structure of coral, only little attention has been paid on the micro scale inside coral polyp. Determining how the carbon concentrations change inside coral polyps is essential to understanding coral biomineralization and coral's tolerance to ocean acidification. In recent decades it has been argued that corals elevate pH and the aragonite saturation state of the calcifying fluid to promote skeleton calcification, which could be enhanced with illumination (Goreau 1959, Carlon 1996, Gattuso et al., 1999). In addition to elevating pH, corals must transport ions from surrounding seawater, such as Ca^{2+}, CO_3^{2-}, and HCO_3^-, to the site of calcification. But neither the source nor the species of these elements have been clearly identified. Coral biomineralization has been studies with limited techniques. Agostini et al., (2012) used a new micro titration method and first measured TA concentrations inside the polyp. They took gastric fluid from dozens of polyps and measured its pH and alkalinity. Their result showed a TA increase in the dark and decrease in the light. But the sampling process of gastric fluid would cause inaccuracy. Microelectrodes were used to measure the ion dynamics inside coral polyps. Al-Horani et al., (2013) built pH and Ca^{2+} electrodes and measured the ion

dynamic inside gastric fluid. However, in order to get a better understanding of carbon system inside coral polyp, we still need one more parameter among CO_3^{2-}, HCO_3^{2-}, pCO_2, and TA. The design of CO_3^{2-} microelectrode by de beer et al., (2008) enabled us to explore the carbon system at the micro space and the new CO_3^{2-} ionophore designed by Lee et al., (2004) provided us a better stability and more accurate result. Therefore, by combining our pH and CO_3^{2-} data, we successfully measured the whole carbonate chemistry inside coral polyp.

Many of the previous studies on models inside coral polyps have been done on photosynthesis, calcification, and their relationship with light (Hohn and Merico, 2012; Kleypas et al., 2011; Watanabe et al., 2013). These models provide an estimate range of coral response to light. However, fewer models have been done on total alkalinity (TA) and dissolved inorganic carbon (DIC) because the lack of experimental data. Nakamura et al., (2013) developed a simulation model that includes both TA and DIC inside the coelenteron and calcifying fluid and the their concentrations change in response to light. But in the model, their initial condition and some parameter values might not be good enough because the lack of directly measured data on TA and DIC inside coral polyps. In this paper, we further developed their model with more parameters and microelectrode-measured data from our own microelectrode work, which provided us more information about chemical compositions at different parts of coral polyp.

2.2 Materials and Methods

2.2.1 Experimental design

2.2.1.1 Corals and maintenance conditions.

Experiments focused on two species of corals: *Orbicella faveolata*, and *Turbinaria reniformis*. *Orbicella faveolata* is the major reef-building species in the Caribbean and *Turbinaria reniformis* is a common Pacific coral species. Both species contain photosynthetic symbionts, often called zooxanthellae, and form an aragonite skeleton. Small pieces of *Orbicella faveolata* were sampled from the Florida Keys and transported to the laboratory in University of Georgia. *Turbinaria reniformis* were collected between 3–10 m depth in northwest Fiji (17°29'19"S, 177°23'39"E) in April 2011 and shipped to Reef Systems Coral Farm in New Albany, OH, prior to shipment to the our lab at the University of Georgia. Corals were acclimated to a laboratory aquarium at 26°C with light levels of about 200 μmol photons /m^2/s for at least two weeks prior to conducting pH and CO_3^{2-} profile measurements.

2.2.1.2 Microelectrodes.

pH microelectrodes (Zhao and Cai, 1999), CO_3^{2-} microelectrodes (Han et al. 2014; de Beer et al., 2008), and Ca^{2+} microelectrodes (de Beer et al., 2000) were constructed as described previously. By changing the temperature of our micro puller, we successfully made microelectrodes with a tip diameter between 10-15 μm, which

enables us to profile into the coral polyp. pH microelectrodes were calibrated with three commercial pH standard buffers(pH=4,7, and 10) at 25 °C.

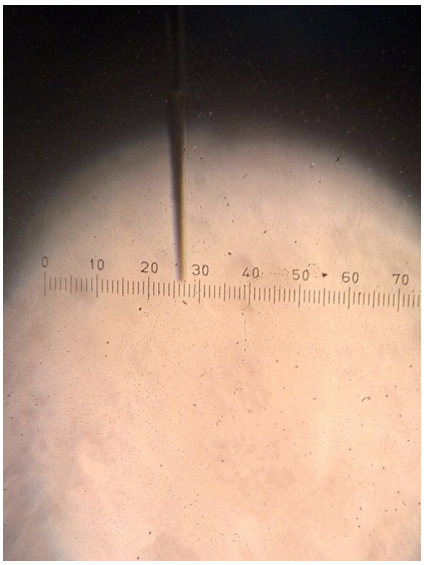

Figure 2-1 pH microelectrode with a tip diameter between 15-20 μm. Microelectrode was photo'd with a 10*40 microscope, each grid is 20 μm.

CO_3^{2-} microelectrodes were made follow Han and de Beer CO_3^{2-} microelectrodes (Han et al. 2014; de Beer et al., 2008), but with different carbonate ionophere that was designed by Lee et al., (2004). CO_3^{2-} microelectrodes were calibrated in CO_3^{2-} standard solutions with five different concentrations ranging from 50 to 500 μmol/L. By adding HCl or $NaHCO_3$ into the seawater we collected from Gulf of Mexico, we shifted the carbonate system of seawater by adjusting the pH. Carbonate concentration gradients were set up at about 50, 150, 250, 350, and 500 μmol/L by controlled amount of HCl and $NaHCO_3$ added. Standard solutions were

then bubbled with air for 24 hours to make sure there is no further exchange of CO_2 with air during the experiment. Finally CO_3^{2-} concentrations were precisely calculated by CO2SYS with total alkalinity and pH measured by Gran titration and Ross electrode.

Ca^{2+} microelectrodes (de Beer et al., 2000) were calibrated with calcium standard solutions (5 mmol/L, 10 mmol/L, 20 mmol/L). To prepare these standard solutions, a known amount of $CaCO_3$ powder was in HCl and diluted with artificial seawater that lacked calcium. Different concentrations were made by serial dilution.

Ag/AgCl wire was used to connect microelectrode and pH meter. To ensure the accuracy of measurement, same Ag/AgCl wire was used for calibration and measurement.

Performances of our microelectrodes are showed in Table 2-1.

Table 2-1 Performances of pH, CO_3^{2-}, and Ca^{2+} microelectrodes.

Microelectrode	Response Range	Slope (mV/pH)	Lifetime (days)	t_{98} (S)	Drift mV/Hour
pH	pH 5.5 - 12	58±2	14	5	0.5
Ca^{2+}	5 - 30 mM	29±1	7	5	0.6
CO_3^{2-}	90 - 300 μM	30±1	3	5	0.5

2.2.1.3 Experiments setup.

A coral fragment was placed in a water bath at 26 °C for microsensor measurements. Artificial seawater was circulated inside water bath cell by a stir bar at

a constant rate. The overlying seawater had a salinity of 35‰, pH 8.2–8.3 and final total alkalinity of approximately 1.8 mmol/L. Light was incident vertically from above using a Fiber-Lite (Dolan-Jenner Industries Inc., USA) at a constant light intensity (500 μmol photons /m^2/s). Microelectrodes were positioned vertically toward the coral polyp by a micromanipulator (Kloehn Co. LTD) that was controlled by a laptop. The output of the pH meter was recorded and analyzed using custom software. With the aid of a microscope, the surface of coral polyp was precisely observed by moving the microelectrode toward the polyp and this depth was marked as 0 depth for later data analysis.

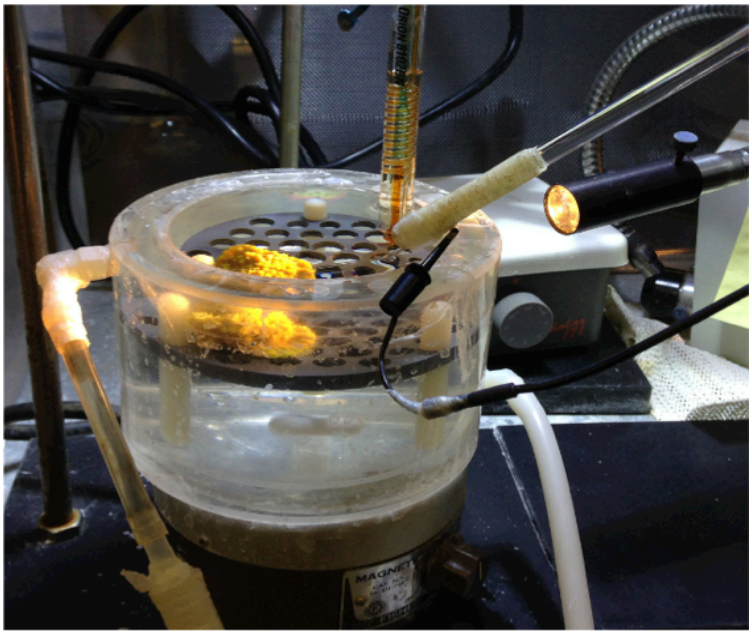

Figure 2-2 Experiment set up. Coral microelectrode setup with the coral *T. reniformis* in the seawater chamber Microelectrode was connected with a pH meter at the right of the figure.

Microelectrodes were stabilized again in the bulk solution and then moved into coral polyp and stopped at a depth of 500 μm. According to our early profiles, this depth could capture a highest photosynthesis rate and would be less affected by tissue movement the locations closer to the surface. The surface position (depth=0) was determined by slowly moving the microelectrode toward coral mouth while observing the coral movement under a microscope. Light intensity was set up as 500 μmol photons /m^2/s and was cycled on and off every ~10 minutes.

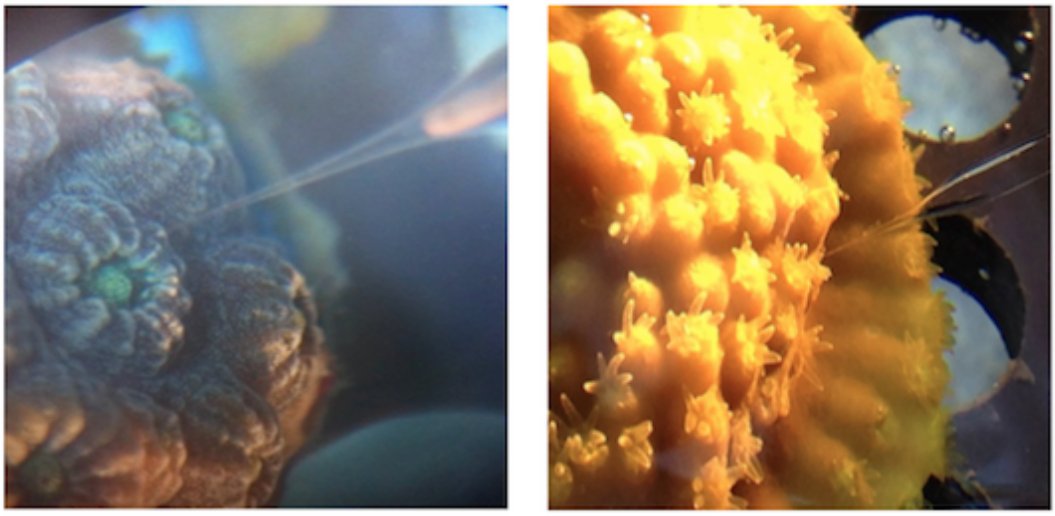

Figure 2-3 Microelectrodes on coral *O. faveolata* (left), and *T. reniformis* (right).

2.2.2 Carbonate chemistry calculation

Measured pH on the NBS scale was converted to the total pH scale using following equation:

$$pH_T = pH_{NBS} - 0.1 \quad \text{[eq 1]}$$

To calculate the carbonate chemistry inside the coral polyp, the measured pH and CO_3^{2-} were used to calculate the other carbonate system parameters. The equations used were as follows with the definition of terms listed in Table 2-2:

$$[CO_{2aq}+H_2CO_3] = [H^+]^2*[CO_3^{2-}]/(K_1*K_2) \quad \text{[eq 2]}$$

$$pCO_2 = [CO_{2aq}+H_2CO_3] /K_H \quad \text{[eq3]}$$

$$DIC = [CO_{2aq}+H_2CO_3] + [HCO_3^-] + [CO_3^{2-}] = [CO_3^{2-}] ([H^+]^2/(K_1*K_2) + [H^+]/K_2 + 1) \quad \text{[eq 4]}$$

$$C\text{-}Alk = [CO_3^{2-}] ([H^+]/K_2 + 2) \quad \text{[eq 5]}$$

$$B\text{-}Alk = [B(OH)_4^-] = T_B*K_B/([H^+]+K_B), \quad \text{[eq 6]}$$

$$TAlk = C\text{-}Alk + B\text{-}Alk \quad \text{[eq 7]}$$

pH and CO_3^{2-} data were recorded every 5 seconds and calculated for average value. TA and DIC were calculated by equation 1-7.

Table 2-2 Definition of terms in equations 1-7.

pH_T	Total pH scale
pH_{NBS}	pH in NBS
T_B	Total B concentration in seawater. (Lee et al., 2010)
$K_{sp\text{-}arag}$	The solubility constant of aragonite
T_B,	Total B concentration in seawater(Lee et al., 2010)
K_B	The dissociation constant of boric acid in seawater
$[CO_{2aq}]$	>99.5% of the total (Morel and Hering, 1992),(Dickson, 1993)
K1	The first dissociation constants of carbonic acid
K2	The second dissociation constants of carbonic acid

2.2.3 Model

2.2.3.1 Overview of the model

This model is based on the ‘‘trans’’ calcification concept (McConnaughey and Falk 1991; McConnaughey and Whelan 1997; Allemand et al., 2004) and modified from Nakamura et al. (2013). Three components of the coral polyp system were included in this model: the ambient seawater, coelenteron and calcifying fluid. But as we only focus on TA and DIC, our model is expressed with six variables: (1) total alkalinity (TA) in the ambient seawater (TA_{amb}); (2) total dissolved inorganic carbon (DIC) in the ambient seawater (DIC_{amb}); (3) TA in the coelenteron (TA_{coe}); (4) DIC in the coelenteron (DIC_{coe}); (5) TA in the calcifying fluid (TA_{cal}); and (6) DIC in the calcifying fluid (DIC_{cal}).

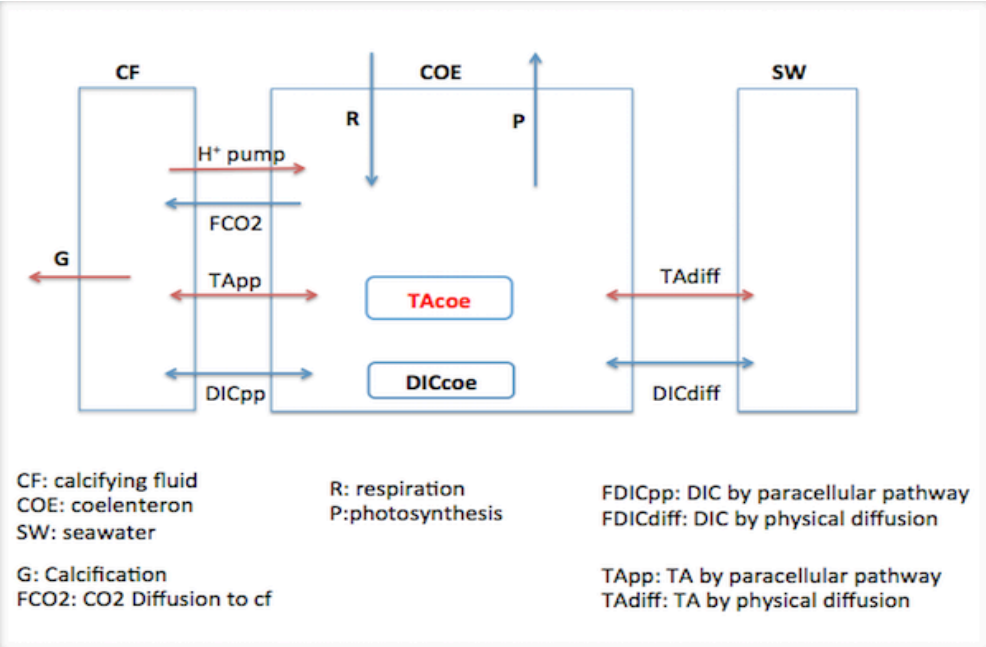

Figure 2-4 A schematic diagram of the coral polyp model. Three compartments and six parameters were used in simulation.

2.2.3.2 Governing equations of the mass conservation model

Calcification, photosynthesis and physical diffusion are the three main processes that affect the TA and DIC in this model. Calcification is the main processes inside the coral that would alter both TA and DIC: when 1 mole of $CaCO_3$ is produced, TA decreases by 2 moles and DIC decreases by 1 mole. The H^+ flux via Ca-ATPase (FH), on the other hand, would only affect the TA: when 1 mole of H^+ is pumped out from calcifying fluid (CF), 1 mole of TA is produced in calcifying space and 1 mole of TA is consumed in the coelenteron. Photosynthesis would alter DIC in coelenteron: when 1 mole C is produced, DIC is decreased by 1. Physical diffusion

also works to affect the chemical concentrations. The diffusion rate is determined by the concentration gradient of different components, and mass transfer coefficients between compartments.

2.2.3.3 Mass balance equation

Inside the calcifying fluid, physical diffusion, calcification and H^+ pump affect the carbon system. Therefore, to summarize all the fluxes, the TA and DIC dynamics in the calcifying fluid are expressed as follows:

$$\frac{dTA_{cal}}{dt} = (-2G + F_H + F_{TA_{pp}})\frac{1}{h_{cal}} \quad \text{[eq 8]}$$

$$\frac{dDIC_{cal}}{dt} = (-G + F_{CO_2} + F_{DIC_{pp}})\frac{1}{h_{cal}} \quad \text{[eq9]}$$

in which G is the calcification rate, F_H is the H^+ flux by H^+ pumping, FTA_{pp} and $FDIC_{pp}$ are TA and DIC fluxes through the paracellular pathway. F_{CO2} is the CO_2 flux from the coelenteron to the calcifying fluid. Values or calculations of the parameters were shown in Table 2-3 and Equations 16-17.

Here we assume the calcification rate and H^+ pump rate are zero in dark because both of these processes requires energy, which is supported by photosynthesis.

Inside the coelenteron, H^+ pumping, physical diffusion with and overlying seawater and exchange through paracellular pathway with calcifying fluid affect the

flux of TA. From Agostini et al., (2012), the release of organic acid also contributes a certain part of TA increase.

$$\frac{dTA_{coe}}{dt} = (-F_H - F_{TA_{pp}} + F_{TA_{diff}})\frac{1}{h_{coe}} \quad \text{[eq10]}$$

$$\frac{dDIC_{coe}}{dt} = (-P + R - F_{CO_2} - F_{DIC_{pp}} + F_{DIC_{diff}} + F_{DIC_{sink}})\frac{1}{h_{coe}} \quad \text{[eq11]}$$

In overlying seawater, because our chamber is an open system, our overlying seawater kept an stable TA and DIC concentrations at 2.4 mmol/L and 1.5 mmol/L.

2.2.3.4 Physical diffusion

The TA, DIC and DO physical diffusion between overlaying seawater and coelenteron through coral polyp mouth are driving by concentration gradient. Positive or negative value indicates the direction of each flux.

The physical diffusion flux are expressed as follows:

$$\begin{aligned} F_{\mathrm{TA\_diff}} &= S(\mathrm{TA_{amb}} - \mathrm{TA_{coe}}), \\ F_{\mathrm{DIC\_diff}} &= S(\mathrm{DIC_{amb}} - \mathrm{DIC_{coe}}) \quad \text{and} \\ F_{\mathrm{DO\_diff}} &= S(\mathrm{DO_{amb}} - \mathrm{DO_{coe}}), \end{aligned} \quad \text{[eq12]}$$

where S is the mass transfer velocity. According to Hearn et al., (2001), S is expressed as following regression equation:

$$S = (65.7\tau^{0.4} + 4.7) \times 10^{-4}, \quad \text{[eq13]}$$

where t is the shear stress and can be calculated by:

$$\tau = \frac{1}{2} C_b U^2 \rho, \quad \text{[eq14]}$$

where ρ is the sea water density and C_b is the bottom drag coefficient, and U is the bulk horizontal current velocity.

Anther diffusion pathway between the coelenteron and the calcifying fluid is molecular CO_2 diffusion across the membrane. The CO_2 flux through the membrane is expressed as the gradient difference between the concentrations of CO_2 in the calcifying fluid and in the coelenteron fluid:

$$F_{CO_2} = k_{CO_2}([CO_2^*]_{coe} - [CO_2^*]_{cal}), \quad \text{[eq15]}$$

where k_{CO2} is the permeability coefficient. The CO_2* values can be calculated from TA and DIC using CO2SYS (Dickson et al., 2007).

2.2.3.5 Paracellular pathway

The transport of TA and DIC between the coelenteron and the calcifying fluid were via the paracellular pathway (FTA_pp and FDIC_pp, respectively). These fluxes are expressed as follows:

$$F_{TA\_pp} = k_{pp}(TA_{coe} - TA_{cal}) \quad \text{and} \quad \text{[eq16]}$$

$$F_{DIC\_pp} = k_{pp}(DIC_{coe} - DIC_{cal}), \quad \text{[eq17]}$$

where kpp is coefficient for the paracellular transport.

2.3 Numerical simulation with the mass conservation model

A central difference scheme is used for converting a differential equation into a set of algebraic equations at each grid point (Boudreau, 1997). The numerical simulation code was written in Matlab. The parameter values and the initial conditions are listed in Tables 2-3 and 2-4. "Profile data" in Table 2-3 and Table 2-4 include both directly measured data from our earlier pH, CO_3^{2-}, and Ca^{2+} profiles with microelectrodes (Cai et al., submitted), and calculated value with Equation 1-7(e.g., calcification rate, TA, and DIC).

Table 2-3 The parameter values used in the model simulations

Symbol	Description	Value	Unit	From
hcoe	Thickness of coelenteron	3000	mm	Profile data
hcal	Thickness of calcifying fluid	10	mm	Profile data
P	Photosynthesis rate	$1.5*10^{-5}$	$mol/m^2/s$	Assumed
R	Respiration rate	$1.4*10^{-5}$	$mol/m^2/s$	Assumed
kpp	Conductivity through the paracellular pathway	$3.0*10^{-10}$	m/s	Tuning
Cb	Bottom drag coefficient	0.01		Reidenbach etal.(2006)
G	Calcification rate	$2.1*10^{-5}$	$mol/m^2/s$	Profile data
F_H	H^+ flux through Ca-ATPase	$2.1*10^{-5}$	$mol/m^2/s$	Tuning

Table 2-4 The initial conditions of the model simulations

Symbol	Description	Value	Unit
TAsw	TA in overlaying seawater	2400	μmol/L
TAcoe	TA in coelenteron	1800	μmol/L
TAcf	TA in calcifying fluid	1500	μmol/L
DICsw	DIC in overlaying seawater	1500	μmol/L
DICcoe	DIC in coelenteron	1400	μmol/L
DICcf	DIC in calcifying fluid	1400	μmol/L

2.4 Result and discussion

2.4.1 pH, CO_3^{2-}, and Ca^{2+} dynamics.

The effects of switching the light on were measured inside coral polyp, at a depth of 500 μm. The pH, CO_3^{2-}, and Ca^{2+} in the gastric cavity exhibited variations in the light (Figure 2-5, Figure 2-6). Ion concentrations changed inside the coral polyp immediately in response to changes in light intensity. After turning on the light, pH and CO_3^{2-} concentrations increased within a few seconds and decreased right after we turned off the light. The Ca^{2+} dynamics showed an opposite pattern, decreasing in the light and increasing in the dark. The concentration changes were about ±0.5 unit-pH for proton, ±100 μmol/L for CO_3^{2-}, and ±1 mM for Ca^{2+}.

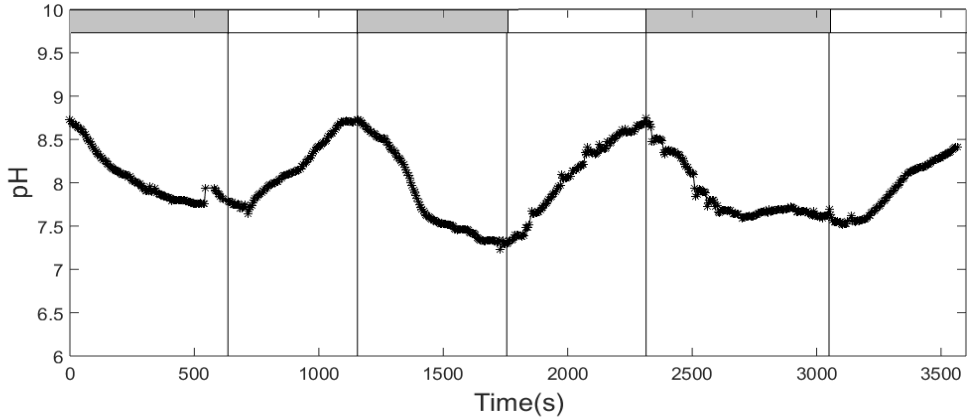
pH
Time(s)

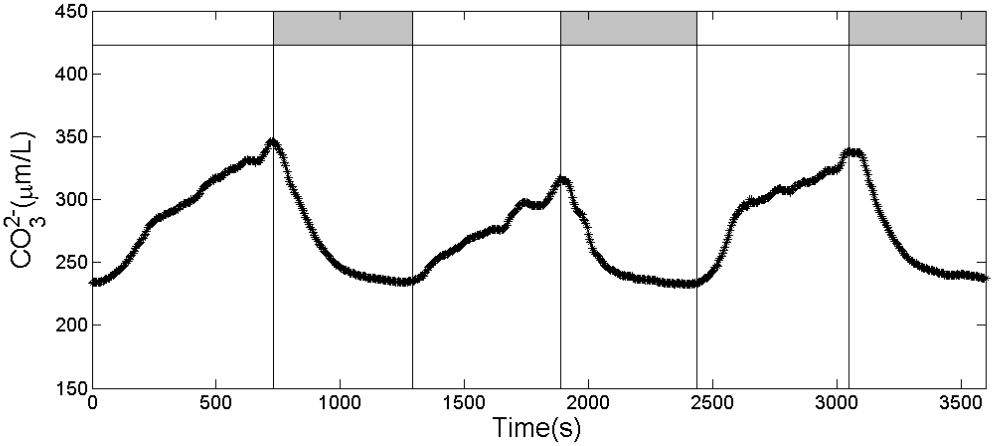
CO_3^{2-}(μm/L)
Time(s)

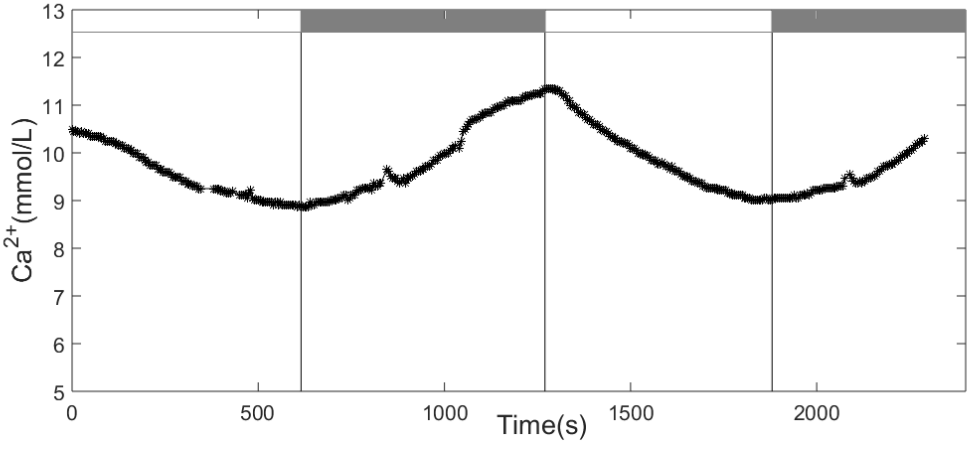
Ca^{2+}(mmol/L)
Time(s)

Figure 2-5 pH, CO_3^{2-}, and Ca^{2+} dynamic on coral *O. faveolata*.

For coral *Orbicella faveolata*, pH increased reaching its highest value at 8.7 during the light and dropping to its lowest point of ~7.5 after 10 min in dark. CO_3^{2-} concentration reached its highest value at ~350 μmol/L after 10 min in light and decreased to ~220 μmol/L in the dark. The calcium concentration decreased in the light due to calcification and it had a minimum value of ~7 mmol/L, and a maximal value at ~10 mmol/L in the dark. For pH and CO_3^{2-} concentrations, the rates of change were not always the same. Most of the time, pH and [CO_3^{2-}] dropped sharply as we turned off the light. But during the light period, the rate is relatively steady. The rates of Ca2+ concentration changes were always approximately the same.

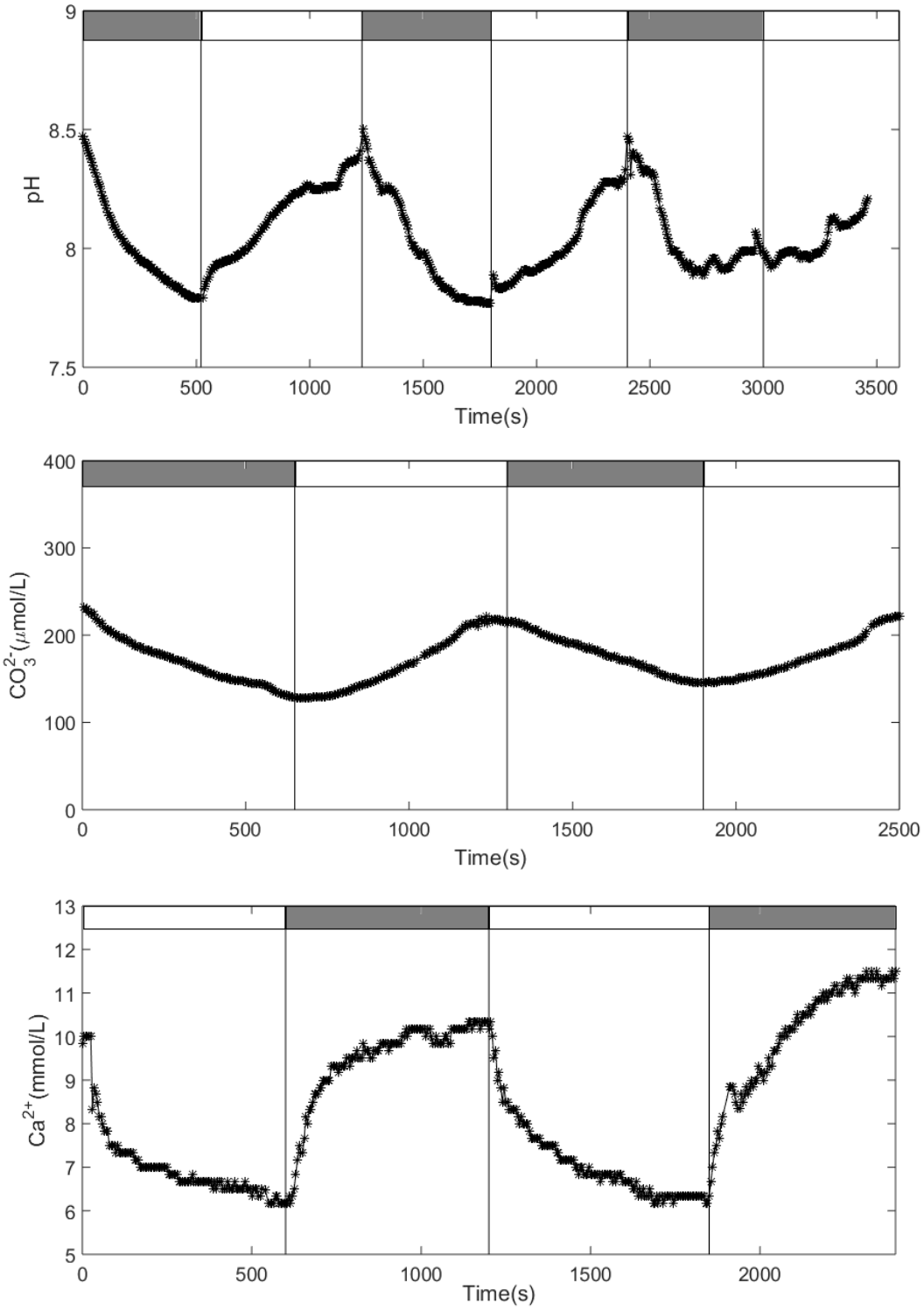

Figure 2-6 pH, [CO_3^{2-}], and [Ca^{2+}] dynamic on coral *T. reinform.*

In *Tubinaria reinformis,* we obtained similar results. The range of pH, [CO_3^{2-}], and [Ca^{2+}] swings between light and dark periods were only slightly different from those observed in *O. faveolata*. Unlike *O. faveolata*, the pH and [CO_3^{2-}] rates of change are relatively steady for *T. reinformis,* which may be a result of the widely opened mouth. But the calcium concentrations changed very rapidly when we turn on/off the light, which indicates the system reached steady state.

2.4.2 Total alkalinity and dissolved inorganic carbon concentrations: experimental data vs simulation result.

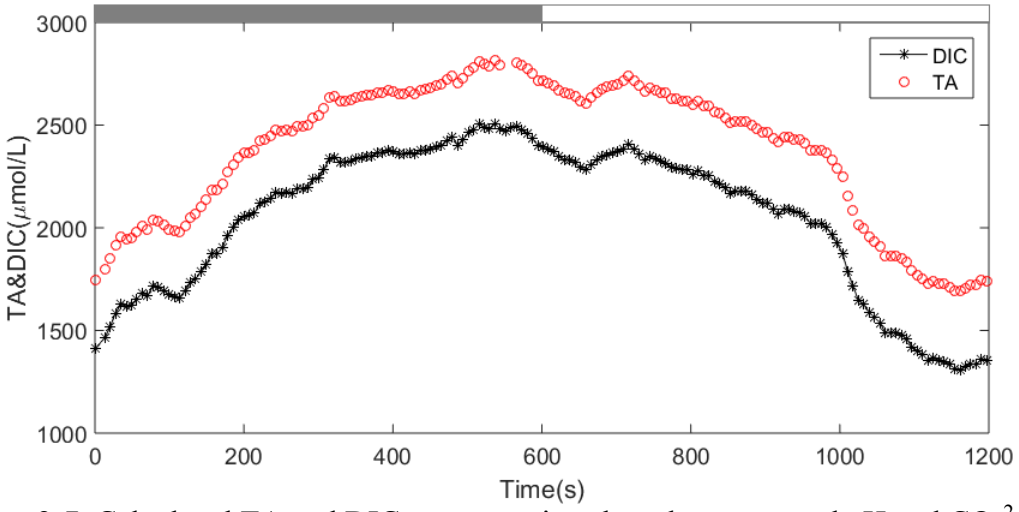

Figure 2-7 Calculated TA and DIC concentrations based on averaged pH and CO_3^{2-} data. 0-600s indicate dark and 600-1200s is in light.

As shown above, our calculated TA and DIC both decreased in light and increased during the dark period. TA increased from ~1800 μmol/L to ~2800 μmol /L

while DIC increased from ~1400 μmol/L to ~2400 μmol/L. The rate of increase was higher at first then became steady as the time approached 10 min. After we turned on the light, TA and DIC both dropped immediately. TA dropped from ~2800 μmol/L to 1800 μmol/L and DIC dropped from ~2400 μmol/L to ~1400 μmol/L. Both of their final values are slightly lower than initial conditions.

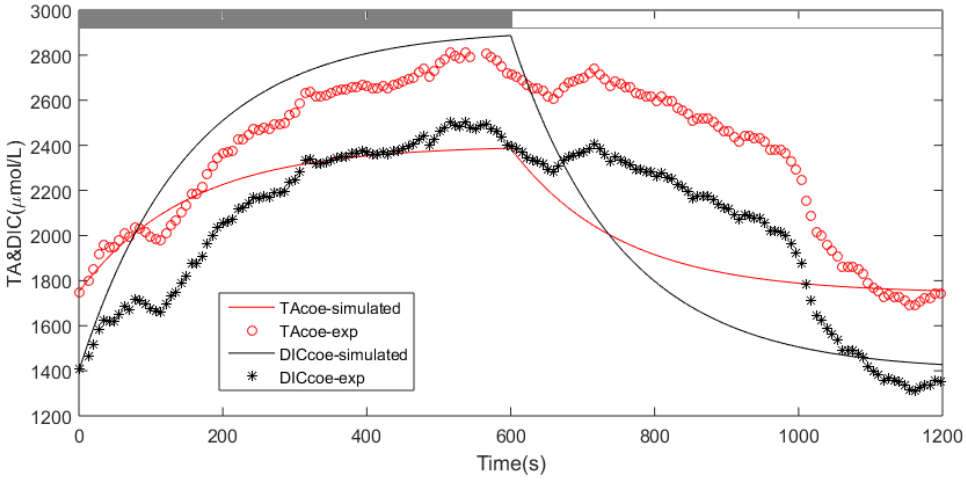

Figure 2-8 Simulation result of TA and DIC in coelenteron verse experimental data. Black star and red cycle are experimental DIC and TA. Black and red lines are the simulated DIC and TA. 0-600 seconds indicate dark and 600-1200 seconds is in light.

The results of our initial simulation are shown in Figure 2-8. TA inside coral coelenteron reached ~2400 μmol/L in dark and went back down to 1800 μmol/L in the light. Similar to TA, DIC reached ~2800 μmol/L in dark and 1400 μmol/L in light. Our modeling results fit with the trend of experimental data but our simulated highest TA is ~400 μmol/L lower than experiment data and the highest modeled DIC is ~300

μmol/L higher. According to our simulation, the TA increase in the dark is due to physical diffusion into the coelenteron from overlying seawater. The DIC increase is due to respiration and diffusion. The rate of increase was fast at the beginning and became slower after the coelenteron TA concentration approached the overlying seawater, a trend that agreed with our experimental data. In the light, our model also showed a shift from rapid concentration changes initially to slower changes reaching a steady-state by approximately 10 min. For both TA and DIC, the concentrations dropped with a high rate immediately because both calcification and physical diffusion favor the decrease trend. As TA and DIC concentrations in the model kept dropping, the coelenteron concentrations approached that of the overlying seawater, which changed the net effect of physical diffusion and caused a lower rate of decrease. But the experimental data showed a steadier rate of decrease, which indicates the present of some factors that prevented the acute concentration change. Here we assume some buffering systems might work to resistant the pH change, and so modifying the rate of change of TA and DIC.

To explain the difference between simulations and experimental data, we considered the following possibilities:

1. Experimental error. According to our model, if there is no extra TA supply at dark, the concentration of coelenteron won't be able to succeed the overlying seawater level, which is 2400 μmol/L for our experiment. But a high coelenteron TA value exceeding that of seawater was also measured by the complimentary micro-

titration technique (Agostini et al., 2012). Beside, the microelectrode technique have been developed and tested for decades and we performed testing and calibration on both pH and [CO_3^{2-}] in every trial. Thus, we have confidence in our data. But corals are living organisms, it's impossible for us to control their inside microenvironment, which may result in slightly difference among coral polyps and there could be mismatch as our pH and [CO_3^{2-}] data were not measured at the same polyp and same time.

2. There might be an unknown TA pool in coelenteron that supplied extra alkalinity. If our experimental TA and DIC are correct, there must be another TA pool during the dark period, which allowed the TA to exceed that of the overlying seawater. Here we posit the presence of an additional "TA pool" and we develop our alkalinity mass balance equations as:

$$\frac{dTA_{cal}}{dt} = (-2G + F_H + F_{TA_{pp}})\frac{1}{h_{cal}} \quad \text{[eq18]}$$

$$\frac{dTA_{coe}}{dt} = \left(-F_H - F_{TA_{pp}} + F_{TA_{diff}} + F_{TA_{pool}}\right)\frac{1}{h_{coe}} \quad \text{[eq19]}$$

Having defined this unknown alkalinity pool, we need to consider its source and whether DIC accompanies TA in this source. Here we considered two different assumptions: i) this TA pool only include inorganic alkalinity; ii) it only include organic alkalinity. As an inorganic TA source, according to Redfield ration, the rate of

TA/DIC change would fit a ration of 17:106, thus $F_{DIC_{pool}} = -\frac{106}{17} * F_{TA_{pool}}$. If this is an inorganic alkalinity source, our DIC mass balance equation will be developed as:

$$\frac{dDIC_{cal}}{dt} = (-G + F_{CO_2} + F_{DIC_{pp}})\frac{1}{h_{cal}} \quad \text{[eq20]}$$

$$\frac{dDIC_{coe}}{dt} = \left(-P + R - F_{CO_2} - F_{DIC_{pp}} + F_{DIC_{diff}} + F_{DIC_{pool}}\right)\frac{1}{h_{coe}} \quad \text{[eq21]}$$

The simulation result for assumption I is shown in Figure 2-9. By tuning the input rate of the TA pool; the TA simulation result successfully fitted our experimental data but the DIC concentration reached a very small value at ~500 μmol/L, which is much too low, so we ruled out assumption I.

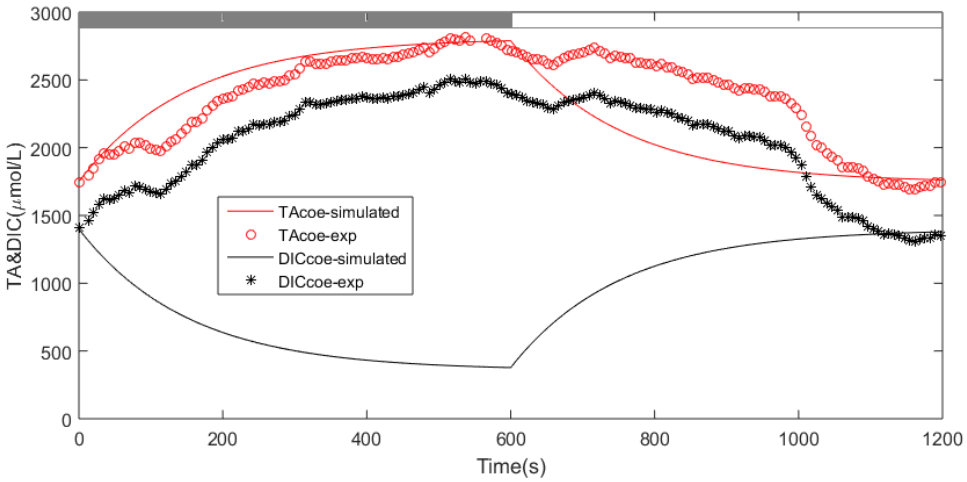

Figure 2-9 Assumption I: Modeling result of TA and DIC in coelenteron verse experimental data. Black star and red cycle are experimental DIC and TA. Black and red lines are the simulated DIC and TA. 0-600 seconds indicate dark and 600-1200 seconds is in light.

If the additional "TA pool" is an organic alkalinity source, it will only affect TA, our DIC mass balance equations still remain the same.

$$\frac{dDIC_{cal}}{dt} = (-G + F_{CO_2} + F_{DIC_{pp}})\frac{1}{h_{cal}} \quad \text{[eq22]}$$

$$\frac{dDIC_{coe}}{dt} = \left(-P + R - F_{CO_2} - F_{DIC_{pp}} + F_{DIC_{diff}}\right)\frac{1}{h_{coe}} \quad \text{[eq23]}$$

Simulation result of assumption II is shown in Figure 2-10. Coelenteron DIC concentration is still lower than expected, but fits better comparing to assumption I, which indicate that this part of unknown TA doesn't come from signal source but comes both organic and inorganic way.

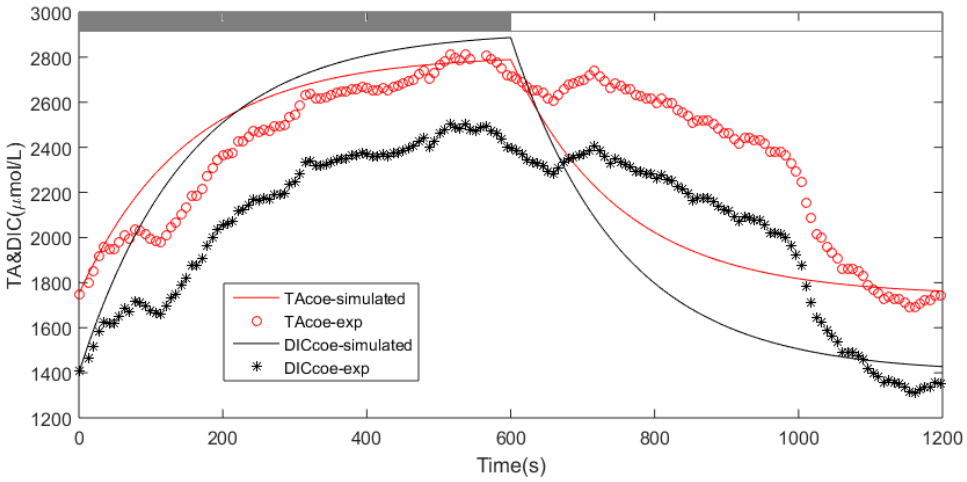

Figure 2-10 Assumption II: Modeling result of TA and DIC in coelenteron verse experimental data. Black star and red cycle are experimental DIC and TA. Black and red lines are the simulated DIC and TA. 0-600 seconds indicate dark and 600-1200 seconds is in light.

By analysis our experimental data, we calculated the ratio of organic and inorganic TA (Figure 2-11). About 40% of TA increase in dark was due to this unknown TA pool and the simulation will perfectly fit our data if 15% of the unknown TA is from an inorganic source.

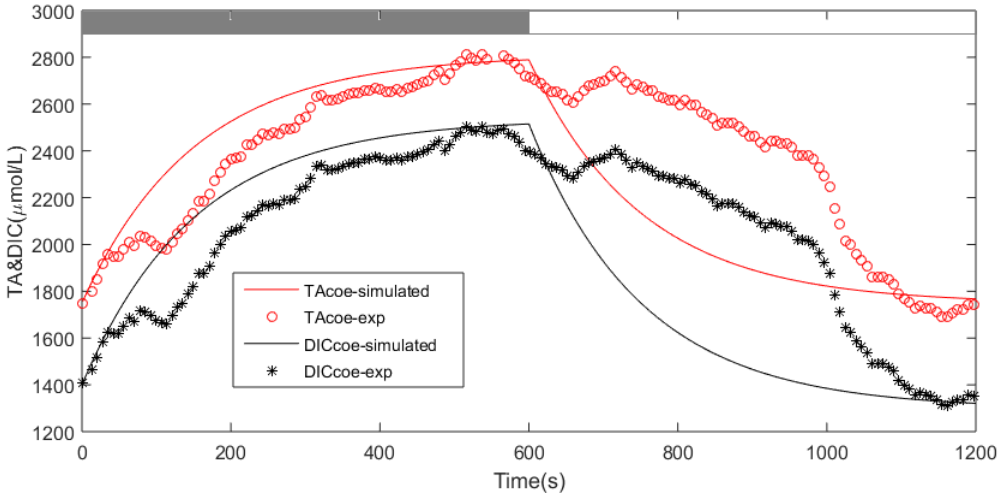

Figure 2-11 Final simulation result: 85% of unknown TA comes from organic sources. Black star and red cycle are experimental DIC and TA. Black and red lines are the simulated DIC and TA. 0-600 seconds indicate dark and 600-1200 seconds is in light.

2.5 Conclusion

This work is the first to successfully measure CO_3^{2-} concentrations inside coral polyps, which enabled the calculation of other parameters in the carbon system. We can only estimate a range of TA and DIC because we can't get both pH and CO_3^{2-} data on a same polyp at the same time, the calculated TA and DIC couldn't be precisely enough. In the next step, we will try to combine pH and CO_3^{2-} electrode together to avoid uncertainty during TA/DIC calculation. However, our data basically fit with earlier micro-titration result by Agostini et al., (2012), in trend and approximate

concentrations, which indicates that our initial measurements of TA/DIC derived from independent pH and CO_3^{2-} profiles were reasonable. In our model, we assumed calcification rate and H^+ flux are zero in dark because of the lack of energy, and consider respiration rate are the same in both light and dark environment. However as much work on "light enhanced calcification" and respiration phenomenon have been conducted, we should find a better way to describe theses variables and have a better understanding of the rate of changes.

Chapter 3

CONCLUSIONS

In this research, we successful measured pH and CO_3^{2-} concentration at different layers of coral polyps with microelectrodes. In chapter 1, we focused on calcifying fluid at a single time point and in chapter 2 we measured one-hour pH and CO_3^{2-} dynamics in coelenteron with light turned on and off.

In chapter 1, our pH and CO_3^{2-} profile data in calcifying fluid supports the H^+ pumping mechanism and the whole carbon system at calcifying fluid were composed with the combined pH and CO_3^{2-} data. Furthermore, with the value of different carbon species, we analysis their sources and find out how coral controlled their inner environment to against ocean acidification.

In chapter 2, the light affected pH, CO_3^{2-}, and Ca^{2+} dynamics in coral coelenteron were measured with microelectrode. Concentrations changes were fit the process of photosynthesis and earlier research. By analyzing pH and CO_3^{2-} concentration change, we got the result of light effected TA and DIC dynamics. A 3-box model was created to analysis the sources of TA and DIC in coelenteron and calculated the rate of different resources.

REFERENCES

Agostini, S. *et al.* Biological and chemical characteristics of the coral gastric cavity. *Coral Reefs* **31**, 147-156, doi:10.1007/s00338-011-0831-6 (2012).

Allemand, D. *et al.* Biomineralisation in reef-building corals: from molecular mechanisms to environmental control. *Comptes Rendus Palevol* **3**, 453-467, doi:http://dx.doi.org/10.1016/j.crpv.2004.07.011 (2004).

Allison, N., Cohen, I., Finch, A. A., Erez, J. & Tudhope, A. W. Corals concentrate dissolved inorganic carbon to facilitate calcification. *Nat Commun* **5**, doi:10.1038/ncomms6741 (2014).

Al-Horani, F. A., Al-Moghrabi, S. M. & de Beer, D. The mechanism of calcification and its relation to photosynthesis and respiration in the scleractinian coral Galaxea fascicularis. *Marine Biology* **142**, 419-426 (2003).

Al-Horani FA., 2005. Effect of changing seawater temperature on photosynthesis and calcification in the scleractinian coral Galaxea fascicularis, measured with O_2, Ca^{2+} and pH micro-sensors. Sci Mar 69:347–354

Barnes, D.J., Chalker, B.E. Calcification and photosynthesis in reef-building corals and algae. In: Dubin- sky, Z. (Ed.), Ecosystems of the World. Coral Reefs, vol. 25. Elsevier, Amsterdam, pp. 109–131. (1990)

Boudreau BP. Diagenetic models and their implementation. Springer, Berlin (1997)

Barnes, D. J. & Devereux, M. J. Productivity and calcification on a coral reef: A survey using pH and oxygen electrode techniques. *Journal of Experimental Marine Biology and Ecology* **79**, 213-231, doi:http://dx.doi.org/10.1016/0022-0981(84)90196-5 (1984).

Cai, W.-J., Zhao, P. & Wang, Y. pH and pCO_2 microelectrodes measurement and diffusive behavior of carbon dioxide species in coastal marine sediments. *Marine Chemistry* **70**, 133-148 (2000).

Carlon DB., 1996. Calcification rates in corals. Science 274:117

Caldeira, K. & Wickett, M. E. Anthropogenic carbon and ocean pH. *Nature* **425**, 365-365 (2003).

Cohen, A. L. & Holcomb, M. Why corals care about ocean acidification: Uncovering the mechanism. *Oceanography* **22**, 118–127, doi:10.5670/oceanog.2009.102 (2009).

Cohen, A. L. & McConnaughey, T. A. Geochemical Perspectives on Coral Mineralization. *Reviews in Mineralogy and Geochemistry* **54**, 151-187, doi:10.2113/0540151 (2003).

de Beer, D. *et al.* A microsensor for carbonate ions suitable for microprofiling in freshwater and saline environments. *Limnology and Oceanography: Methods* **6**, 532-541 (2008).

Dickson AG., Sabine CL., Christian JR (eds) ., 2007. Guide to best practices for ocean CO_2 measurements. PICES special publica- tion 3:191

Dickson, A.G., 1993. pH buffers for sea water media based on the total hydrogen ion concentration scale. Deep-Sea Res., 40: 107-118.

Frankignoulle M., Gattuso J., Biondo R., Bourge I., Copin-Monte´gut G., Pichon M., 1996. Carbon fluxes in coral reefs. II. Eulerian study of inorganic carbon dynamics and measurement of air-sea CO_2 exchanges. Mar Ecol Prog Ser 145:123–132

Gagnon, A. C., Adkins, J. F. & Erez, J. Seawater transport during coral biomineralization. *Earth and Planetary Science Letters* **329–330**, 150-161, doi:http://dx.doi.org/10.1016/j.epsl.2012.03.005 (2012).

Gattuso, J.-P., Allemand, D., and Frankignoulle, M.,1999. Photosynthesis and calcification at cellular, organismal and community levels in coral reefs: A review on interactions and control by carbonate chemistry. *Am. Zool*. 39, 160–183.

Gattuso J., Pichon M., Delesalle B., Canon C., Frankignoulle M., 1996. Carbon fluxes in coral reefs. I. Lagrangian measurement of community metabolism and resulting air-sea CO_2 disequilibrium. Mar Ecol Prog Ser 145:109–121

Goreau, T. F., 1959. The physiology of skeleton formation in corals. I. A method for measuring the rate of calcium deposition by corals under different conditions. *Biol. Bull.* 116, 59–75.

Han, C., Cai, W.-J., Wang, Y., Ye, Y., 2014. Calibration and evaluation of a carbonate microsensor for studies of the marine inorganic carbon system. Journal of Oceanography, 70(5): 425-433.

Hoegh-Guldberg, O. & Bruno, J. F. The Impact of Climate Change on the World's Marine Ecosystems. *Science* **328**, 1523-1528, doi:10.1126/science.1189930 (2010).

Hearn CJ., Atkinson MJ., Falter JL., 2001. A physical derivation of nutrient-uptake rates in coral reefs: effects of roughness and waves. Coral Reefs 20:347–356.

Holcomb, M. *et al.* Coral calcifying fluid pH dictates response to ocean acidification. *Sci. Rep.* **4**, doi:10.1038/srep05207 (2014).

Hohn, S. & Merico, A. Modelling coral polyp calcification in relation to ocean acidification. *Biogeosciences* **9**, 4441-4454, doi:10.5194/bg-9-4441-2012 (2012).

Johnston IS., 1980. The ultrastructure of skeletogenesis in zooxanthellate corals. Int Rev Cytol 67: 171–214.

Langdon, C. *et al.* Effect of elevated CO_2 on the community metabolism of an experimental coral reef. *Global Biogeochem. Cycles* (2003).

Lee, B.H., Y. Shim and S.B. Park, A lipophilic sol-gel matrix for the development of a carbonate-selective electrode. Analytical chemistry, 2004. 76(20): p. 6150-6155

Lee, K. et al., 2010. The universal ratio of boron to chlorinity for the North Pacific and North Atlantic oceans. Geochimica et Cosmochimica Acta, 74(6): 1801-1811.

Li, Y. H. & Gregory, S. Diffusion of ions in sea water and in deep-sea sediments. *Geochimica et Cosmochimica Acta* **38**, 703 (1974).

Kuhl, M., Cohen, Y., Dalsgaard, T., Jergensenl, B. & Revsbech, N. Microenvironment and photosynthesis of zooxanthellae in scleractinian corals studied with microsensors for 02, pH and light. *Marine ecology progress series* **117**, 159-172.1995 (1995).

Kleypas JA., Anthony KRN., Gattuso J-P., 2011. Coral reefs modify their seawater carbon chemistry - case study from a barrier reef (Moorea, French Polynesia). Global Change Biol 17: 3667–3678 .

McConnaughey TA., Falk RH., 1991. Calcium-proton exchange during algal calcification. Biol Bull 180:185–195

McConnaughey TA., Whelan JF., 1997. Calcification generates protons for nutrient and bicarbonate uptake. Earth-Sci Rev 42:95–117

Morel, F.M.M., Hering, J.G., 1992. Principles and Applications of Aquatic Chemistry. John Wiley and Sons, New York, 588 pp.

Nakamura, T., Nadaoka, K., Watanabe, A., 2013. A coral polyp model of photosynthesis, respiration and calcification incorporating a transcellular ion transport mechanism. Coral Reefs, 32(3): 779-794.

Orr, J. C. *et al.* Anthropogenic ocean acidification over the twenty-first century and its impact on calcifying organisms. *Nature* **437**, 681-686, doi:http://www.nature.com/nature/journal/v437/n7059/suppinfo/nature04095_S1.html (2005).

Reidenbach MA., Monismith SG., Koseff JR., Yahel G., Genin A., 2006. Boundary layer turbulence and flow structure over a fringing coral reef. Limnol Oceanogr 51:1956–1968

Ries, J. B. A physicochemical framework for interpreting the biological calcification response to CO2-induced ocean acidification. *Geochimica et Cosmochimica Acta* **75**, 4053-4064, doi:http://dx.doi.org/10.1016/j.gca.2011.04.025 (2011).

Sabine, et al. 2004. The oceanic sink for anthropogenic CO_2. Science 305: 367–371, doi:10.1126/science.1097403

Shamberger, K. E. F. *et al.* Diverse coral communities in naturally acidified waters of a Western Pacific reef. *Geophysical Research Letters* **41**, 499-504, doi:10.1002/2013GL058489 (2014).

Sültemeyer, D. & Rinast, K.-A. The CO_2 permeability of the plasma membrane of Chlamydomonas reinhardtii: mass-spectrometric ^{18}O-exchange measurements from $^{13}C^{18}O_2$ in suspensions of carbonic anhydrase-loaded plasma-membrane vesicles. *Planta* **200**, 358-368, doi:10.1007/BF00200304 (1996).

Tambutté, S. *et al.* Coral biomineralization: From the gene to the environment. *Journal of Experimental Marine Biology and Ecology* **408**, 58-78, doi:http://dx.doi.org/10.1016/j.jembe.2011.07.026 (2011).

Watanabe A., Yamamoto T., Nadaoka K., Maeda Y., Miyajima T., Tanaka Y., Blanco AC., 2013. Spatiotemporal variations in CO_2 flux in a fringing reef simulated using a novel carbonate system dynamics model. Coral Reefs 32:239–254.

Venn, A., Tambutté, E., Holcomb, M., Allemand, D. & Tambutté, S. Live Tissue Imaging Shows Reef Corals Elevate pH under Their Calcifying Tissue Relative to Seawater. *PLoS ONE* **6**, e20013, doi:10.1371/journal.pone.0020013 (2011).

Zhao, P., Cai, W.-J., 1999. pH polymeric membrane microelectrodes based on neutral carriers and their application in aquatic environments. Anal. Chim Acta, 395: 285-291.

Appendix A

SUPPLEMENTARY MATERIALS

I. Sample collection and maintenance

The measurements focused on three species of corals: *Orbicella faveolata, Turbinaria reniformis* and *Acropora millepora*. All species contain photosynthetic endosymbionts, often called zooxanthellae (*Symbiodinium* spp.), and form an aragonite skeleton. Small fragments of *Orbicella faveolata* were sampled from the Florida Keys (GPS coordinates) in month/year from xx depth and transported to the laboratory in University of Georgia (Florida Keys National Marine Sanctuary permit 2014-015). *Turbinaria reniformis* and *Acropora millepora* were collected between 3–10 m depth in northwest Fiji (17°29'19"S, 177°23'39"E) in April 2011 and shipped to Reef Systems Coral Farm in New Albany, OH, where they were maintained in recirculating indoor aquaria with natural light (greenhouse, 700–1000 μmol quanta m^{-2} s^{-1}) and commercially available artificial seawater (Instant Ocean Reef Crystals) for at least 2 weeks before shipping to the Cai lab at the University of Georgia. Corals were acclimated to a closed-system laboratory aquarium with artificial seawater at 26°C with light levels of about 200 μmol photons /m^2/s for at least two weeks prior to conducting pH and CO_3^{2-} profile measurements. Fragments of same species were collect from the same coral colonies.

II. Microelectrode construction and properties

pH microelectrodes (Cai et al., 2000; Zhao and Cai, 1999) and CO_3^{2-} microelectrodes (de Beer et al., 2008; Han et al., 2014) were constructed as previously described. We made our microelectrodes with a tip diameter between 10-15 μm (Figure A1), which enabled us to make pH measurements along a profile into the coral polyp. pH microelectrodes were calibrated with three commercial pH NBS standard buffers (pH=4,7, and 10) at 26 °C.

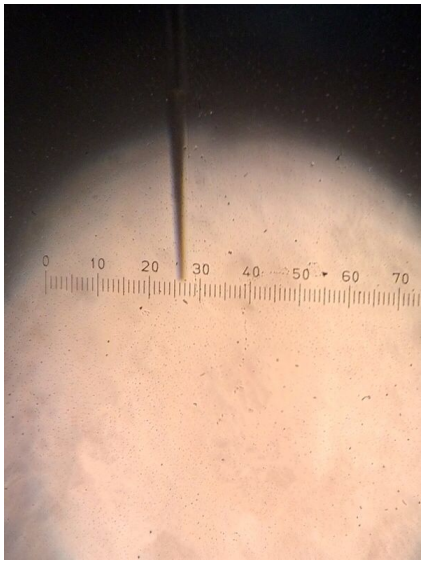

Figure A1. pH microelectrode with a tip diameter between 15-20 μm. The microelectrode was photographed at 400x under a dissecting microscope. Note the microelectrode tip is flat and thus the vertical sensing resolution is believe to be only a few μm.

CO_3^{2-} microelectrodes were calibrated in CO_3^{2-} standard solutions (Han et al., 2014). Carbonate concentrations were set at approximately 50, 150, 250, 350, and 500 μmol/L by adding controlled amounts of HCl and $NaHCO_3$ into filtered seawater collected from the Gulf of Mexico. Standard solutions were then bubbled with air for 24 hours to minimize further exchange of CO_2 with air during the experiment. Finally, CO_3^{2-} concentrations were precisely calculated by CO2SYS with total alkalinity and pH measured by Gran titration and a Ross electrode, respectively.

III. Coral microelectrode measurement setup and microelectrode stability

For each coral microprofile, a coral was placed in the microelectrode setup chamber (Figure A2) under 500 μmol photons /m^2/s of light in recirculating artificial seawater that was maintained under conditions shown in Tables A1, A2 and A3 for a maximum of 20-60 minutes. A stir bar provided seawater mixing within the chamber and a combination glass electrode was used to provide a reference pH and to monitor pH change in the water. During profile measurements, a calibrated Orion Ross glass electrode (NBS scale buffer solutions, 4.01, 7.00 and 10.01) was used in the overlying water as a reference. The microelectrode was inserted directly into a polyp mouth and advanced at 5 to 50 μm increments. Repeated pH profiles in the same coral polyp were highly reproducible (Figure A3a, b).

As with the pH profiles, during initial work, CO_3^{2-} microelectrodes were inserted into each polyp twice (Figure A4). At the end of the 1st insertion, the electrode was retrieved back to the overlying water and read the same (previous) value. Even though the coral contracted (in this example, the zero depth moved downward) due to the microprobe insertion causing some variability in CO_3^{2-} profiles, duplicate profiles on the same polyp were highly reproducible over 30-60 minutes.

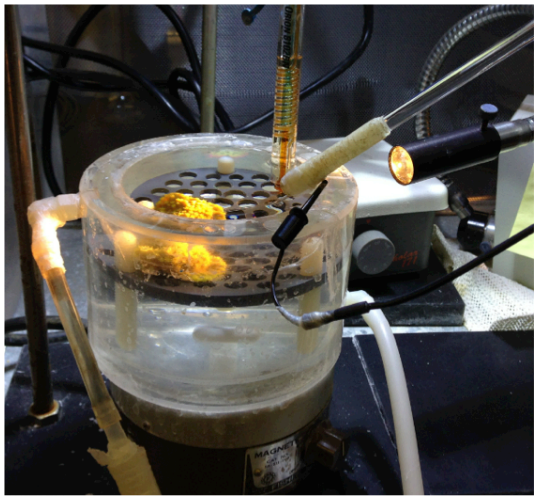

Figure A2 Coral microelectrode setup with the coral *Turbinaria reniformis* in the seawater chamber.

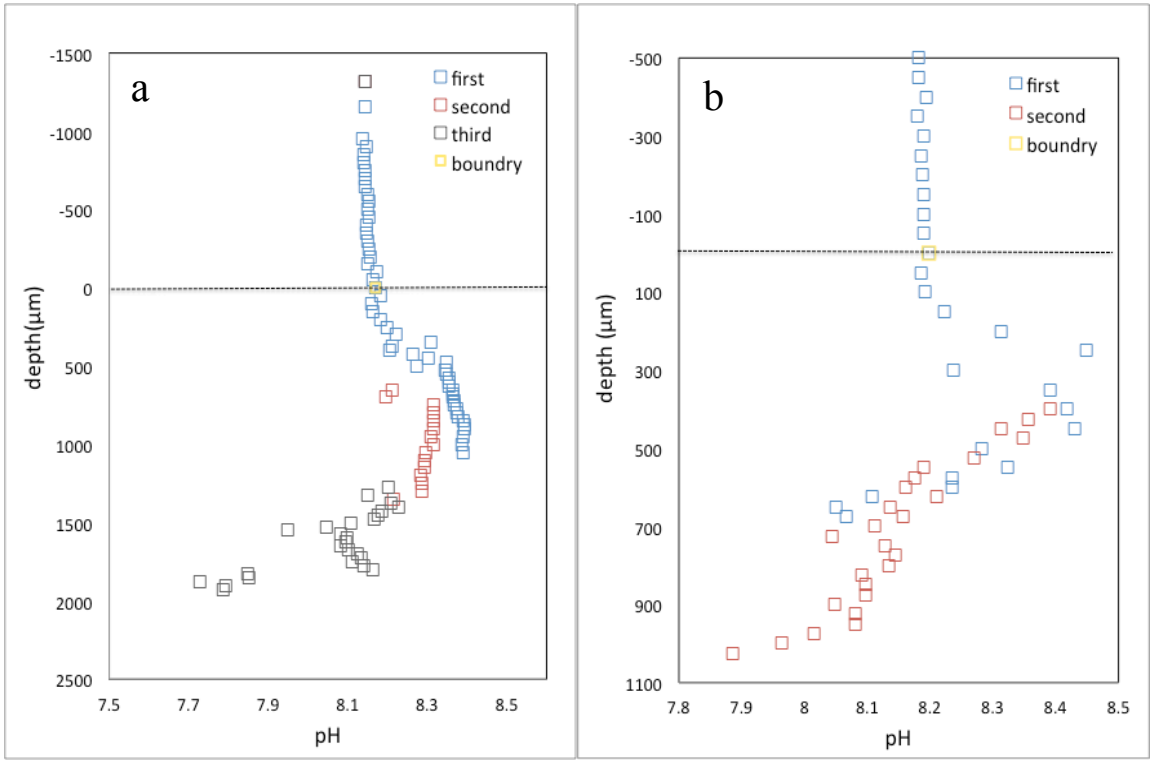

Figure A3 pH microelectrode electrode performance and stability test, showing repeated pH_{NBS} microelectrode profile readings inside a *T. reniformis* (a) and *A. millepora* (b) coral polyp. Repeated profiles are listed as first (blue), second (red), and third (gray). The boundary between the coral mouth and seawater is shown with a dashed line bisected by a yellow square.

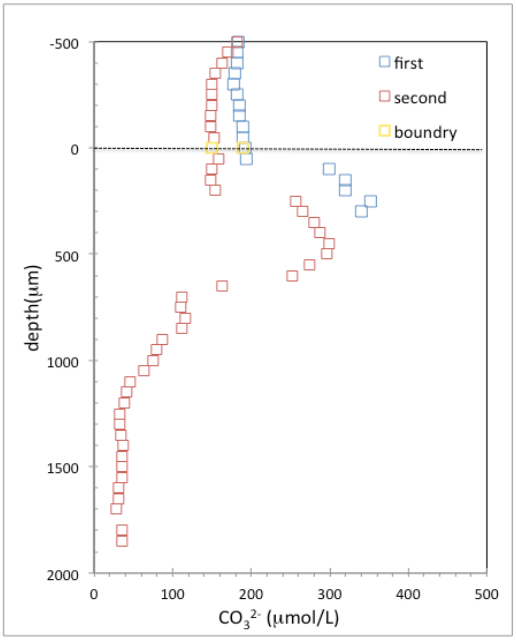

Figure A4 Duplicate CO_3^{2-} microelectrode profiles on *T. reniformis.* At the second insert, the polyp contracted, and thus the interface moved down. If the depths are adjusted, the two profiles are highly repeatable. Repeated profiles are listed as first (blue) and second (red). The boundary between the coral mouth and seawater is shown with a dashed line bisected by a yellow square.

Table A1 _Measurement conditions for each pH_{NBS} and CO_3^{2-} profile for the coral *Orbicella faveolata.*

	Date	Salinity	pH	T (°C)	TA (mmol/L)
pH1	04/22/2013	35.5	8.26	26.0	1.790
pH 2	05/07/2013	35.0	8.19	26.0	1.701
CO_3^{2-}	08/18/2013	35.0	8.17	26.0	1.700

Table A2 Measurement conditions for each pH_{NBS} and CO_3^{2-} profile for the coral *Turbinaria reniformis*

	Date	Salinity	pH	T (°C)	TA (mmol/L)
pH1	01/09/2015	35.0	8.17	26.0	1.790
pH2	10/07/2012	35.0	8.01	26.0	2.040
CO_3^{2-} 1	07/11/2013	35.5	8.30	26.0	1.690
CO_3^{2-} 2	05/15/2013	35.0	8.24	26.0	2.087

Table A3 Measurement conditions for each pH_{NBS} and CO_3^{2-} profile for the coral *Acropora millepora.*

	Date	Salinity	pH	T (°C)	TA (mmol/L)
pH	09/20/2012	35.0	8.30	26.0	1.790
CO_3^{2-}	08/01/2013	35.0	8.10	26.0	1.611

IV. pH and carbonate chemistry inside the coral polyp

Measured pH on the NBS scale was converted to the total pH scale using methods described in Dickson (1993) where roughly,

$$pH_T = pH_{NBS} - 0.1 \quad \text{[eq 1]}$$

To calculate the carbonate chemistry inside the coral polyp, the measured pH and CO_3^{2-} were used to calculate the other carbonate species. The equations used were as follows with the definition of terms listed in Table A4:

$$[CO_{2aq}+H_2CO_3] = [H^+]^2*[CO_3^{2-}]/(K_1*K_2) \quad \text{[eq 2]}$$

Note in the main text, $[CO_{2aq}+H_2CO_3]$ are simply given as $[CO_2]$.

$$pCO_2 = [CO_{2aq}+H_2CO_3] /K_H \quad \text{[eq3]}$$

$$DIC = [CO_{2aq}+H_2CO_3] + [HCO_3^-] + [CO_3^{2-}] = [CO_3^{2-}] ([H^+]^2/(K_1*K_2) + [H^+]/K_2 + 1) \quad \text{[eq 4]}$$

$$C\text{-}Alk = [CO_3^{2-}]\ ([H^+]/K_2 + 2) \quad \text{[eq 5]}$$

$$B\text{-}Alk = [B(OH)_4^-] = T_B * K_B/([H^+]+K_B), \quad \text{[eq 6]}$$

$$TAlk = C\text{-}Alk + B\text{-}Alk \quad \text{[eq 7]}$$

$$\Omega_{arag} = [Ca^{2+}][\ CO_3^{2-}]/K_{sp\text{-}arag}, \quad \text{[eq 8]}$$

Table A4 Definition of terms in equations 1-8

pH_T	pH on the total scale
pH_{NBS}	pH on the NBS scale
T_B	Total B concentration in seawater (Lee et al., 2010)
$K_{sp\text{-}arag}$	The solubility constant of aragonite
T_B	Total B concentration in seawater (Lee et al., 2010)
K_B	The dissociation constant of boric acid in seawater
$[CO_{2aq}]$	Aqueous CO_2, >99.5% of the total molecular CO_2 (Morel and Hering, 1992) (Dickson, 1993).
K_1	The first dissociation constants of carbonic acid
K_2	The second dissociation constants of carbonic acid

Average carbonate chemistry values were calculated for the overlying seawater, upper coelenteron (the upper quarter of a profile, ~300-500 μm deep), and bottom of the coelenteron (the bottom quarter of a profile) (Table A5). Based on these findings, likely combinations of carbonate chemistry for the calcifying fluid were calculated by equations 1-8 (Table A4).

Next, using the calculated $[CO_2]$ gradient from Table A5, CO_2 flux (F_{CO_2}) from the coelenteron into the calcifying fluid was calculated using two methods. Note the $[CO_2]$ gradient determined by the microelectrode data (Table A5) is not affected much by the uncertainty caused by relatively large pH and $[CO_3^{2-}]$ ranges inside the calcifying fluid as $[CO_2]$ is nearly 0 (that is an uncertainty of $[CO_2]$ between 0.5 and 0.1 μmol/kg only changes $[CO_2]$ gradient from 29.9 to 30.3 μmol/kg). The two methods are described in the main text (Methods).

Table A5. pH, $[CO_3^{2-}]$, DIC, TAlk, $[CO_2]$ (in μmol/kg), pCO_2, and Ω_{arag} values inside an average coral polyp (data were averaged for all three species in Fig. 2 across their relative depth profiles). Upper coelenteron is the first quarter of a profile where a larger pH and CO_3^{2-} increase were observed, usually at 300-500 μm. Bottom coelenteron is the last quarter of a profile, usually 0-500 mm above the calcifying fluid. CO_2 flux calculation (see methods below) into the calcification layer is calculated based on data in the two highlighted rows.

Zone	pH	$[CO_3^{2-}]$	DIC	TAlk	$[CO_{2aq}]$	pCO_2	Ω_{arag}
Seawater	8.2	183	1479	1759	6.95	252	2.92
Upper coelenteron	8.5	320	1453	1937	3.05	111	5.10
Bottom coelenteron	**7.7**	**80**	**1893**	**1982**	**30.4**	**1100**	**1.28**
Likely combinations of the calcifying fluid	8.7	500	1616	2330	1.90	68.7	7.97
	8.9	700	1685	2649	1.06	38.3	11.2
	9.1	**900**	**1699**	**2907**	**0.54**	**19.6**	**14.3**
	9.5	1100	1489	2962	0.10	3.80	17.5
	10.2	1400	1271	3318	0.01	0.19	22.3

CO_2 flux over 100 or 50 μm distance (mmol $m^{-2}d^{-1}$)	51.5-103.0 5.15-10.3	
Or μmol $cm^{-2}d^{-1}$	217-433	
Or nmol $cm^{-2}h^{-1}$		

Appendix B

PERMISSION LETTER

UNIVERSITY OF DELAWARE | College of Earth, Ocean, & Environment
SCHOOL OF MARINE SCIENCE & POLICY

University of Delaware
Newark, DE 19716-3501
Phone: 302-831-2839
Email: wcai@udel.edu

November 20, 2015

This is to confirm that I give my permission that Yuening Ma can use the manuscript entitled **"Microelectrode characterization of coral interior pH and carbonate chemistry"** as a chapter (chapter 1) in her Master Thesis. She is the second author of this manuscript that is under review by the journal *Nature Communication* (under revision).

Wei-Jun Cai
Professor of Oceanography
Mary A.S. Lighthipe Chair of Earth, Ocean and Environment